JPL Publication 87-32

Final Report on the First Flight of the ATMOS Instrument During the Spacelab 3 Mission, April 29 Through May 6, 1985

Crofton B. Farmer
Odell F. Raper
Fred G. O'Callaghan

October 1, 1987

NASA

National Aeronautics and
Space Administration

Jet Propulsion Laboratory
California Institute of Technology
Pasadena, California

The research described in this publication was carried out by the Jet Propulsion Laboratory, California Institute of Technology, under a contract with the National Aeronautics and Space Administration.

Contents

Contents (Contd)

Figures (contd)

Figures (contd)

Tables

Abstract

The Atmospheric Trace Molecule Spectroscopy (ATMOS) investigation is an experiment utilizing a fast Fourier transform (FFT) interferometer operating in the near- and middle-infrared region of the spectrum to detect as many as possible of the neutral molecular constituents in the Earth's upper atmosphere and to determine their vertical and horizontal distributions. Flown for the first time aboard the shuttle Challenger as a part of Spacelab 3, the experiment measures the radiation from the Sun during those periods in the orbit when the rays from the Sun to the instrument are passing through the Earth's atmosphere (i.e., sunsets and sunrises as seen from the orbiter). During these periods, interferograms are generated at the rate of one each second which yield, when transformed, high resolution (0.01 cm^{-1}) spectra covering the 2.2 to 16 micron region of the infrared. Twenty such occultations were recorded during the Spacelab 3 flight, which have produced concentration profiles for a large number of minor and trace upper atmospheric species in both the Northern and Southern Hemisphere. Several of these species have not previously been observed in spectroscopic data.

In the present report, the underlying rationale and the implementation of the ATMOS investigation are discussed, a description of the sensor is given, and the ground tests and integration procedures leading to the Spacelab 3 flight are described. The data reduction and analysis procedures used after the flight are discussed, a number of examples of the spectra obtained are shown, and the concentration profiles as a function of altitude for the minor and trace gases measured during the mission are presented.

On the basis of the instrument's ability to survive both the launch and the reentry of the shuttle and its flawless performance while on orbit, the concepts involved in the investigation have been proved by the Spacelab 3 flight, and an extended series of reflights are currently being planned as a part of the Atmospheric Laboratory for Applications and Science (ATLAS) Missions. The goals for the investigation during these missions are also discussed.

Section I
Introduction and Scope

The Spacelab investigation entitled Atmospheric Trace Molecule Spectroscopy (ATMOS) was designed to obtain fundamental information related to the chemistry and physics of the Earth's upper atmosphere using the techniques of infrared absorption spectroscopy. There are two principal objectives to be met, the first of which is the determination of the compositional structure of the upper atmosphere and its spatial variability. The determination of this variability establishes the characteristic residence times for the upper atmospheric constituents, the magnitudes of their sources and sinks, and ultimately an understanding of their effects on the stability of the stratosphere. The second objective is to provide the high-resolution, calibrated spectral information needed for the detailed design of more specific instruments for subsequent monitoring of those species found to be critical to atmospheric stability. These spectra will also provide a data base for comparison with future measurements to assess long-term changes in upper atmospheric composition.

This report describes the rationale behind the ATMOS investigation, the strategy adopted for its implementation, the configuration of the sensor that was developed for acquiring the necessary data, and the results from the first ATMOS mission on Spacelab 3 (SL-3). A list of the acronyms used in the report can be found in the Glossary.

A. Experiment Rationale

Over the past decade, as our understanding of the physics and chemistry of the Earth's upper atmosphere has progressed, the need for precise, simultaneous measurements of the spatial and temporal variability of certain groups of key species and related physical properties has become evident. Such measurements, made with a single instrument, eliminate much of the uncertainty that arises when the behavior of these species is assessed by means of measurements made with different instruments at different times and places. Since most of the molecules of interest have active infrared transitions, infrared spectroscopy has proved to be the most useful method for making simultaneous measurements. In order to acquire the data with the required spectral and spatial resolution, atmospheric spectroscopists have made increasing use of the advantages of Fast Fourier Transform (FFT) techniques. The measurements, which are usually made in absorption using the rising or setting Sun as the radiation source, provide profiles of concentration up to the altitude of the measurement platform.

As the measurement programs continued, it became increasingly apparent that radiative transfer and photodissociation processes occurring in the very high regions of the atmosphere (i.e., in the mesosphere and thermosphere) were inextricably linked to the chemistry of the stratosphere and that the measurements needed to be extended into these regions. Again, it was important that these measurements be made in context with the distributions of the key species at the lower altitudes. These regions of the atmosphere are above the altitudes achievable with balloons, and while some very high resolution instruments are capable of obtaining distribution information for individual species above the altitude from which the measurements are made, these instruments cannot obtain the required simultaneous coverage of related groups of molecular species. The obvious solution for extending the altitude region over which simultaneous measurements could be made was the use of FFT techniques from space. This was the underlying rationale for the ATMOS experiment. An additional advantage gained by operating from space is the opportunity to obtain global coverage.

B. Science Objectives and Experiment Implementation

1. Objectives

Since concerns were initially expressed regarding anthropogenically induced modifications to the Earth's ozone layer, photochemists, experimentalists, and modelers have made considerable progress in their efforts to characterize the upper atmosphere and the processes occurring there. Lists of potential reactions have been compiled beginning with estimated or measured distributions of key species (e.g., $CFCl_3$, CF_2Cl_2, CCl_4, N_2O, and H_2O). Rate constants for a large number of these have been measured or remeasured in the laboratory. Through the application of these reaction schemes, intermediate and sink species have been identified, and first-order predictions have been made with regard to their distributions and variabilities. Experimentalists in turn have devised techniques for making the measurements needed to test the model predictions. The entire process has been an iterative one and has progressed to the point where good agreement exists between modeled and measured values for many of the minor and trace constituents of the upper atmosphere; however, there are still a number of discrepancies between measured and modeled values as well as between the results obtained by different techniques applied to the same molecules.

The primary objective of the ATMOS experiment is to measure simultaneously as many of the minor and trace species as possible and to determine their spatial distribution. The simultaneity of the measurements is an important aspect of the experiment by virtue of the highly interactive nature of the photochemical processes that occur in the upper atmosphere. To modelers attempting to predict the effects of the Cl cycle, for example, simultaneous measurements of as many chlorine compounds as possible, together with measurements of the natural minor and trace species, are of far greater benefit than indirectly related individual measurements of chlorine species made at different times and locations. In some cases, the ratios of certain gases are also useful. The HF/HCl ratio, for example, provides information on the partitioning of the photolysis products from the chlorofluorocarbons (CFCs), among other stratospheric species, and also provides some insight into the amount of chlorine derived from sources other than the industrial CFCs. Another relationship of interest is the sum of CH_4 and H_2O. Models predict a decrease in CH_4 with altitude as a result of chemical reactions that are stoichiometrically equivalent to the oxidation of CH_4 to CO_2 with the concomitant production of two molecules of H_2O. Thus, the mixing ratio for H_2O should increase with altitude at twice the falloff rate for CH_4. Some recent measurements for H_2O, however, have shown larger increases in H_2O with altitude than can be accounted for by methane oxidation, and if these measurements are correct, other sources of stratospheric water vapor must be identified.

Another primary objective for acquiring these spectra is to provide a comprehensive data base against which measurements from future flights can be assessed for any long-term changes in upper atmospheric composition. A spectral atlas of the upper atmosphere covering the 2.5- to 16-μm region is being prepared using the data that is currently available from the first flight and will be available to the atmospheric science community. This atlas represents the first input to a data base against which future spectra will be compared.

The ATMOS spectra contain a wealth of additional information regarding upper atmospheric and solar physics, the retrieval of which represents an important secondary objective of the experiment. With appropriate reduction and analysis of the data, information has been extracted relative to temperature profiles, upper atmospheric winds, departures from thermodynamic equilibrium, photolysis thresholds, solar photospheric physics, and many other questions of scientific interest. Since a large number of the spectra returned by the experiment were purely solar (i.e., contain no terrestrial atmospheric features), an opportunity to prepare a high-resolution, high signal-to-noise solar spectrum covering the entire 2.5- to 16-μm wavelength region of the infrared has presented itself.

2. Implementation

In the measurement programs currently under way, experimentalists have employed several remote sensing methods that include quite different techniques: spectroscopy at visible and infrared wavelengths by both absorption and emission; broadband and correlation filter radiometry (infrared, principally in emission); laser heterodyne radiometry and Lidar; and microwave sounding. Observations are made from the ground, from aircraft, balloon, and rocket platforms, and from satellites.

The principal distinction between the methods lies in the effect of spectral resolution on the manner in which altitude information can be extracted from the measurements. The fixed-frequency, very high resolution methods (which include microwave sounding and laser heterodyne techniques) can measure the detailed line shape of a constituent of interest; by appropriate deconvolution methods, the distribution of the constituent above the observation base can be determined, with a vertical resolution approximately equal to the atmospheric scale height. The distribution can be obtained in this case from a single observation at a zenith angle of less than 90 deg. By contrast, the "incoherent" methods (e.g., high-resolution spectroscopy and correlation radiometry) derive the required altitude weighting by recording sequences of measurements at angles greater than 90 deg (limb techniques) and by deconvolving the data using a variety of inversion procedures (often referred to as "onion-peel" methods). For these techniques, therefore, the maximum altitude to which the concentration profile can be determined is the altitude of the observation platform.

A second important distinction regarding remote sensing techniques can be made between emission and absorption measurements. Most high-resolution spectroscopic observations, which have provided data for a large number of the infrared-active constituents of the upper atmosphere, have been made in the absorption mode; such measurements use the Sun as the radiation source, the geometric weighting being obtained by recording spectra during sunset or sunrise. A major disadvantage of spectroscopic or radiometric methods in absorption lies in the fact that measurements can be made only at two rather restrictive times of day. This aspect presents serious difficulties in the case of the diurnally varying species, especially those whose concentrations vary rapidly in response to insolation changes. The latter restriction does not apply, of course, to measurements of the total column and its variation with latitude and season (i.e., where the vertical distribution is not required). Against this, the absorption measurements are not dependent (to the first order) on a detailed knowledge of the temperature along the line of sight of the observations, as is the case for measurements made in emission. In the latter case, errors resulting from uncertainty in temperature depend on detailed factors related to the distribution of the species being measured and can become large when the thermal contrast is small over the region in which the spectral lines are formed.

All the remote methods are subject in some degree to errors arising from uncertainty in the observational geometry, but this is more particularly the case for the limb techniques. As a result of the strong dependence of the line of sight airmass on zenith angle for angles greater than 90 deg, errors in the observation altitude and zenith angle can introduce errors as large as 30% in the deduced molecular column density. The effects of finite beam size and uncertainty in the detailed instrument field of view (FOV) further contribute to this source of error. A second factor common to all the remote methods is the error introduced by uncertainties in the intrinsic molecular line or band parameters for the transitions being observed. For the better-studied molecules (CH_4, N_2O, and H_2O, for example) such errors should not now exceed 5%. However, the more recently emerging species of interest, particularly those that are reactive under laboratory conditions (e.g., $HOCl$), may not be quantitatively understood to better than 50%. A related potential source of systematic differences common to remote measurements of a given molecular constituent is the lack of knowledge of the detailed line shapes under collision-broadened conditions. Depending on the sign of the departure from ideal, pure Lorentzian shape, an error from this source can introduce a skew toward high or low concentrations with respect to the true values at progressively lower tangent height altitudes of observation. In most cases, systematic errors arising from factors related to radiative transfer assumptions in the data reduction process should not exceed 10%.

A characteristic of remote sensing spectroscopic methods is their high specificity; provided that adequate laboratory calibration has been carried out, there is usually no ambiguity associated with the identification and measurement of a given species. Against this, the spatial resolution of remote sensing techniques is very coarse (kilometers). Limb observations, for example, typically sample a volume of atmosphere weighted toward the tangent point at a distance of hundreds of kilometers from the observation platform, with a height (thickness) of 1 or 2 km at the limb. Thus, the effects of spatial and temporal variability must be carefully considered in the interpretation of remotely measured profiles. The remote methods all determine the line of sight column density under one or more geometric path conditions. These values are then converted by geometric and spectral models to average local concentrations at a number of altitudes corresponding to the number of independent measurements acquired.

The choice of the remote sensing method for the ATMOS experiment was dictated by the need to obtain simultaneous high-resolution spectral information for a large number of upper atmospheric species whose transition frequencies are spread throughout the near and middle regions of the infrared. Figure 1 shows several computer-generated low-resolution spectra covering the absorption frequencies for those minor and trace species of interest to the investigation. An additional constraint is the speed with which the data must be acquired; the rapid rates of solar occultation from a Shuttle orbit require that measurements be made at intervals of about 2 seconds. Interferometry, with its high throughput and multiplexing advantages, is the only infrared technique capable of satisfying these constraints.

The ability to detect trace quantities of gases using spectroscopic techniques depends on three factors: (1) the quantities of the gases present in the optical path, (2) the oscillator strengths associated with their spectral features, and (3) the spectral background against which the measurements must be made. The practical limit associated with the detection of a given species is established by these three factors plus the signal-to-noise performance and spectral resolution of the sensor used for the measurements. The resolution requirement for the instrument can be calculated through the establishment of a minimum detection limit criterion and through the

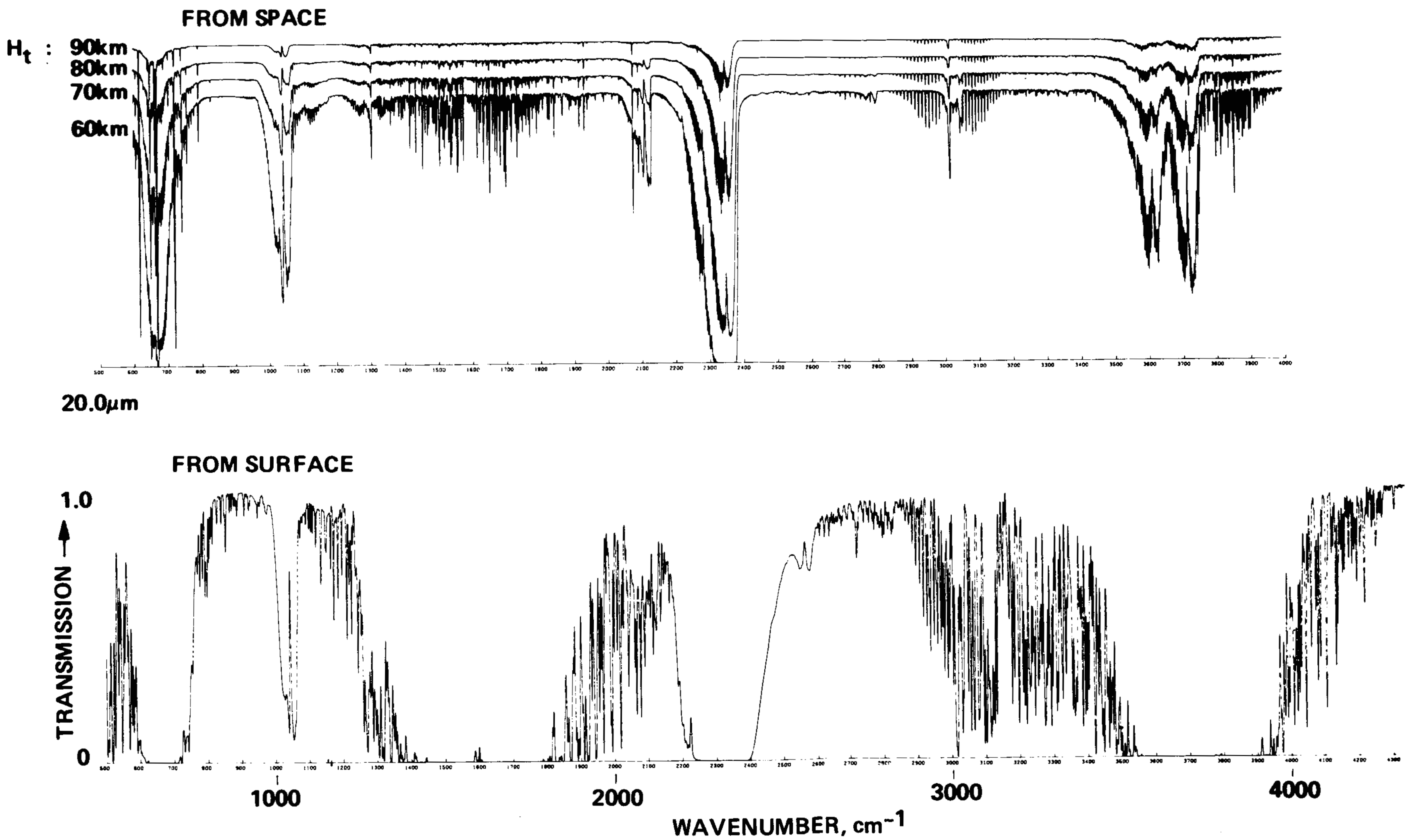

Fig. 1. Synthetic spectra simulating the appearance of the atmosphere from various tangent altitudes from space and from the ground in the infrared wavelength regions covered by the ATMOS instrument.

assumption of realistic line strengths and signal-to-noise performance. The spectral resolution of 0.01 cm^{-1} for the ATMOS sensor was determined through the use of a detection criterion set at 1/10th of the expected concentration of the least abundant species with a signal-to-noise ratio of 100:1 in the final spectra.

The scan time for the instrument was established by the need for a useful vertical resolution in the sampling intervals of the measurements. From modeling considerations, it was determined that the sampling interval should not exceed half a scale height, or about 4 km. Since occultation rates on the Shuttle are typically 1.5 to 2 km/s, a scan time of 2 s was arrived at. To reduce the smearing effects of the changing air-mass on the interferogram, the instrument was actually implemented such that a two-sided interferogram was produced every two seconds with the zero path difference position at the center of the scan.

Covering the entire 2.5- to 16-μm region at 0.01 cm^{-1} resolution every scan is impracticable from the standpoint of both instrument performance and data rate. Thus, the science team selected a set of optical filters covering narrower-wavelength regions for use with the ATMOS instrument. The filters were chosen to be compatible with the alias limits associated with sampling at every second or third fringe of a Helium-Neon (HeNe) reference laser. The wavelength regions covered by the four primary filters are given in Table 1, which also lists the molecules whose infrared transitions occur within each frequency interval.

Two other filters (filters 5 and 6, not shown in Table 1), were also chosen by the ATMOS Science Team for the first Spacelab flight. Filter 6 covered the wavelength region from 650 to 3600 cm^{-1} at relatively low signal-to-noise; it was used to acquire solar spectra, where the opportunity exists to average several hundred identical interferograms during the data reduction process. Filter 5 was specifically designed to cover the CO_2 fundamental bands at 677 cm^{-1} and 2349 cm^{-1} for temperature sounding and Local Thermodynamic Equilibrium (LTE) studies. For compatibility with the instrument's two electrical filters, all the optical filters except filter 4 are used

Table 1. Transmission regions for the ATMOS optical filters showing the principal species to be measured in each region.

Band 1 600–1200 cm^{-1}	Band 2 1100–2000 cm^{-1}	Band 3 1580–3400 cm^{-1}	Band 4 3100–4700 cm^{-1}
CO_2	CO_2	CO_2	CO_2
H_2O	CH_4	CO	H_2O
O_3	H_2O	CH_4	
		H_2O	
		O_3	HF
NH_3		N_2O	HCN
HNO_2	H_2O_2		
HNO_3	HO_2		
HNO_4		NO	
	NO	NO_2	
CCl_3F	NO_2		
CCl_2F_2	N_2O_5	HDO	
CH_3CClF_2	HNO_3	H_2O_2	
CH_3Cl		H_2CO	
CCl_4	HOCl		
COF_2	CF_4	HCl	
COClF		CH_3Cl	
ClO	SO_2		
$ClONO_2$		OCS	
		HCN	

at a sampling rate corresponding to every second HeNe laser fringe. Filter 4 is thus the only filter currently used at the three-fringe sampling rate.

The ATMOS science team developed a strategy for the sequential use of these filters during the first ATMOS flight to ensure that sufficient data was recorded to meet all the primary and secondary objectives of the experiment. This strategy is discussed later in the description of the first flight. The following section describes the instrument designed to meet the functional requirements imposed by the experiment objectives and the adopted approach.

Section II
ATMOS Instrument Development and Testing

A. Background

The ATMOS investigation represents the outgrowth of an atmospheric measurement program begun at the Jet Propulsion Laboratory (JPL) in 1972 using a flight-model High-Speed Interferometer (HSI) designed and built by the Laboratory for use on aircraft and balloon-borne platforms. The original instrument, designated the Mark I, covered the wavelength region from 1.8 to 5.2 μm with an unapodized resolution of 0.125 wave numbers. This instrument, which was flown on a wide variety of aircraft and balloon-borne platforms, gathered information on the mixing ratios of atmospheric minor and trace species from ground level to a height of 40 km. Among these measurements were several stratospheric "firsts," including the first spectroscopic detection of NO, the first NO/NO_2 ratio, the first spectroscopic detection of HC1, the first HF/HC1 ratio, and the first profile for HF in the 20- to 40-km region of the atmosphere.

During the 1976–1977 time period, a Shuttle Definition Study was conducted both to determine the feasibility of acquiring infrared interferometric data from the Space Shuttle and to provide a conceptual design for an instrument capable of making the measurements. This study culminated with the award of a contract to Honeywell Electro-Optics Center (HEOC) in January 1978 to design and build the ATMOS sensor. The following paragraphs describe the design and development of the ATMOS instrument by HEOC.

B. Instrument Overview

A block diagram of the functional elements of the ATMOS instrument is shown in Fig. 2. Radiation enters the instrument via a suntracker and a foreoptics subsystem, with the latter defining the FOV and the size of the beam. The energy rejected by the field stop is reflected to a frame camera and is recorded as an image of the Sun with the position of the FOV of the instrument superimposed. The wave front passing through the field stop is divided by the beamsplitter and modulated by the moving elements in the interferometer. The modulated radiation leaving the beamsplitter passes through one of the six selectable bandpass filters and is focused on a Mercury-Cadmium-Telluride (HgCdTe) detector operating at 77 K.

The signal produced at the detector is conditioned and digitized by the Signal Handling Subsystem (SHSS). The digitized signal is then formatted by the Data Handling Subsystem (DHSS) into a Pulse Code Modulated (PCM) data stream. This signal is then output to the instrument Ground Support Equipment (GSE) or, during a flight, directly to the Shuttle High Rate Multiplexer (HRM). Additional engineering and housekeeping data is processed by the Engineering Data Handling Subsystem (EDHSS) and is output as a part of the high-rate data stream as well as in a separate low-rate engineering stream. All command and control functions for the instrument are performed by the Command and Control Interface Subsystem (CCISS).

C. Instrument Description

For purposes of discussion, the ATMOS instrument, shown in Fig. 3, can be divided into two sections: (1) the optical sensor, composed of all the optical subsystems and the scan servo control unit, and (2) the electronic assemblies, including the compressor for the detector cooler. All the elements of the optical sensor are mounted to an aluminum baseplate that in turn is mounted via vibration isolators to a substructure assembly. This assembly attaches to, but is thermally isolated from, a platform located in the payload cargo bay of

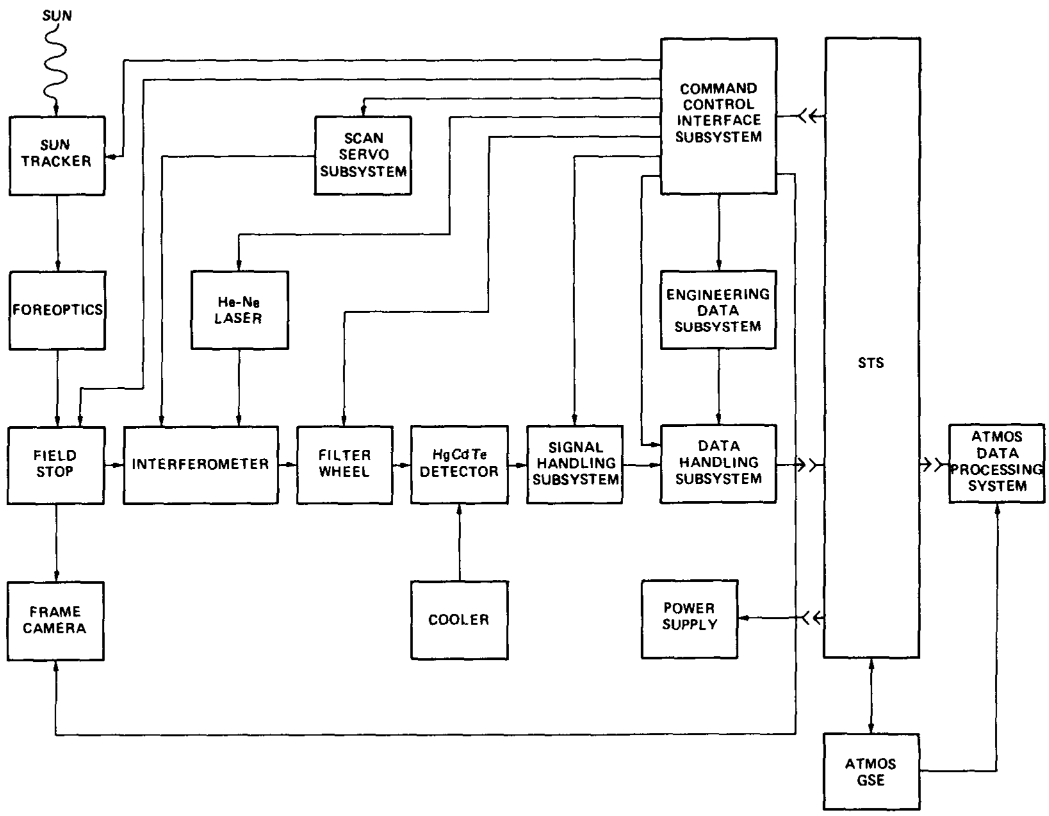

Fig. 2. Block diagram of the ATMOS sensor.

the Shuttle. An aluminum cover, which also mounts to the baseplate, encloses all but the suntracker and camera. The internal pressure of the sensor is maintained at ambient through a vent that is fitted with a desiccant filter assembly designed to provide a clean, dry environment under all conditions.

The electronics section is mounted on a secondary support platform that is mechanically isolated from the main support structure via vibration isolators. The electronics are physically separated into two units, one chassis containing the SHSS, DHSS, EDHSS, and CCISS and the other containing the power supply subsystem. A thermal control plate mounts to the underside of the secondary platform and provides a nominal thermal operating range of +5°C to +45°C under pallet conditions ranging from −150°C to +120°C.

1. Suntracker and Foreoptics

The optical layout for the suntracker and foreoptics, including the frame camera optics, is shown in Fig. 4. The two-axis servo-controlled suntracker tracks the Sun to an accuracy of 0.4 mr with a stability of 0.06 mr. Sun detection and positive feedback are provided by a silicon quadrant array with an acceptance cone angle of 20 deg. In the tracking mode, the sensor's FOV is centered on the solar disk; however, commands can be sent to offset the tracker null position in 1-mr steps to avoid (or seek out) sunspot activity. The tracker can be prepositioned to intercept the Sun at the appropriate time for a subsequent sunset or sunrise encounter by a commandable pointing capability that provides near-hemispheric coverage.

Energy reflected by the suntracker passes through a Zinc Selenide (ZnSe) window and enters the foreoptics. The cover window is Anti-Reflective (AR) coated for improved efficiency in the 2- to 16-μm region without significant loss at the camera wavelength of 0.575 μm. The foreoptics telescope has a 7.5-cm-diameter collecting aperture and consists of two confocal F/3 off-axis paraboloids with a selectable field stop located at their common focus. Field stops corresponding to instrument FOVs of 1, 2, and 4 mr can be selected. Energy passing through the stop is recollimated by the telescope secondary and transferred to the interferometer. Angular magnification is restricted to 2.6 because of obliquity limitations within the interferometer. The rejected energy is reflected to the frame camera via an ellipsoidal mirror. One solar image is recorded by the camera at the end of each 100-cm scan.

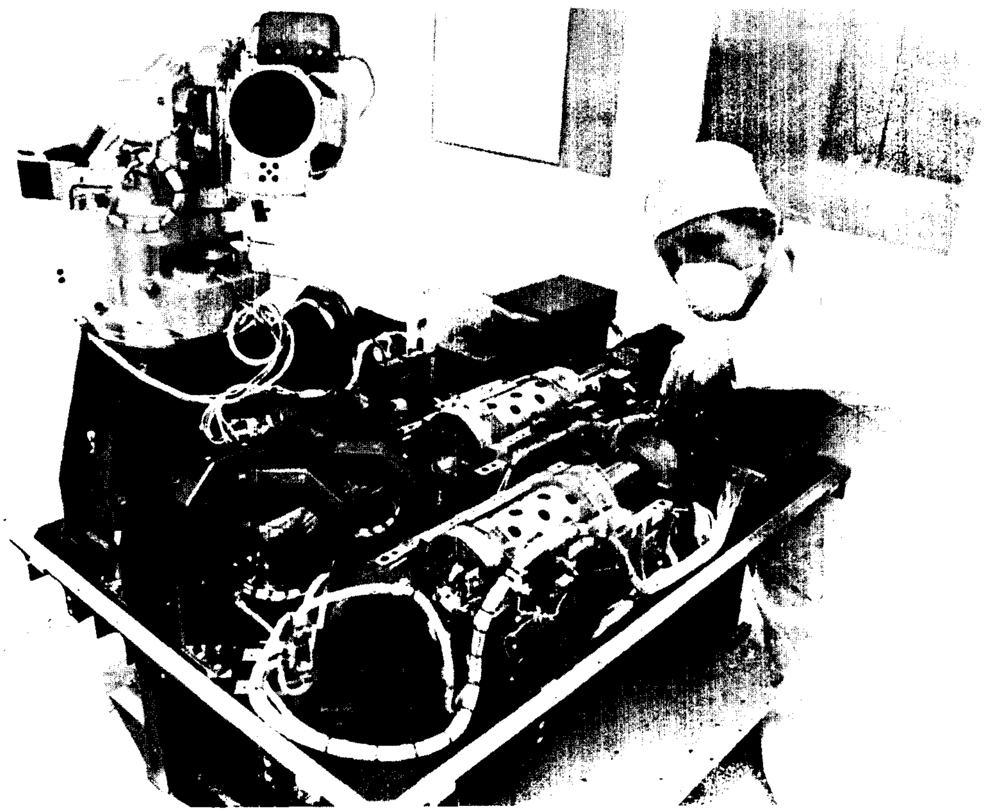

Fig. 3. A cover-off photograph of the ATMOS instrument taken during the final stages of its assembly at Honeywell Electro-Optics Center.

2. Interferometer

A block diagram of the optical layout of the interferometer is also shown in Fig. 4. The optical system is a modified version of the classic Michelson interferometer that uses cat's-eye retroreflectors in place of plane mirrors and double-passing techniques for maximum alignment stability. The design relaxes component alignment tolerances from a few arc seconds to several arc minutes, thus rendering the instrument insensitive to mechanically or thermally induced misalignments.

Energy enters the interferometer through an aperture in the common retro mirror and impinges on the beamsplitter at an angle of incidence of 45 deg. The beamsplitter substrate is Potassium Bromide (KBr) with a Ge/KRS-5 coating designed for optimum efficiency over the 2- to 16-μm region. Radiation reflected from the beamsplitter passes through a KBr compensator plate and goes to the cat's-eye retroreflector, which consists of an F/2.7-paraboloid primary and a slightly convex secondary. The radiation exits the cat's-eye displaced, travels through the compensator, and is reflected off a gold-coated area on the beamsplitter substrate that directs the energy to the retro mirror. The reflected beam then retraces its path back to the beamsplitter surface. The radiation transmitted by the beamsplitter follows a similar path but uses the beamsplitter substrate in transmission rather than in reflection. The Optical Path Difference (OPD) is varied continuously from +50 cm to −50 cm at a retardation rate of 50 cm/s by moving both cat's-eyes equal distances in opposite directions. This has two advantages over a single-moving-element system: first, it decreases the mechanical scan rate to 6.25 cm/s, half its former value; and second, by scanning the cat's-eyes in opposite directions, it rejects common-mode forces, thus providing for a first-order velocity correction. Requirements for high-spectral data quality dictate precision control of the OPD scan to a velocity uniformity of 0.1% peak to peak. This level of performance is achieved through the use of a frequency-stabilized HeNe laser for OPD velocity feedback. The reference laser used in the ATMOS interferometer is a modified Hewlett Packard HP5501A Zeeman split actively stabilized laser providing single-mode, single-frequency output at 0.6330 μm. The laser energy passes through the interferometer parallel to the infrared beam.

The key elements of the scan servo subsystem are shown in Fig. 5. The velocity servo is implemented with two control

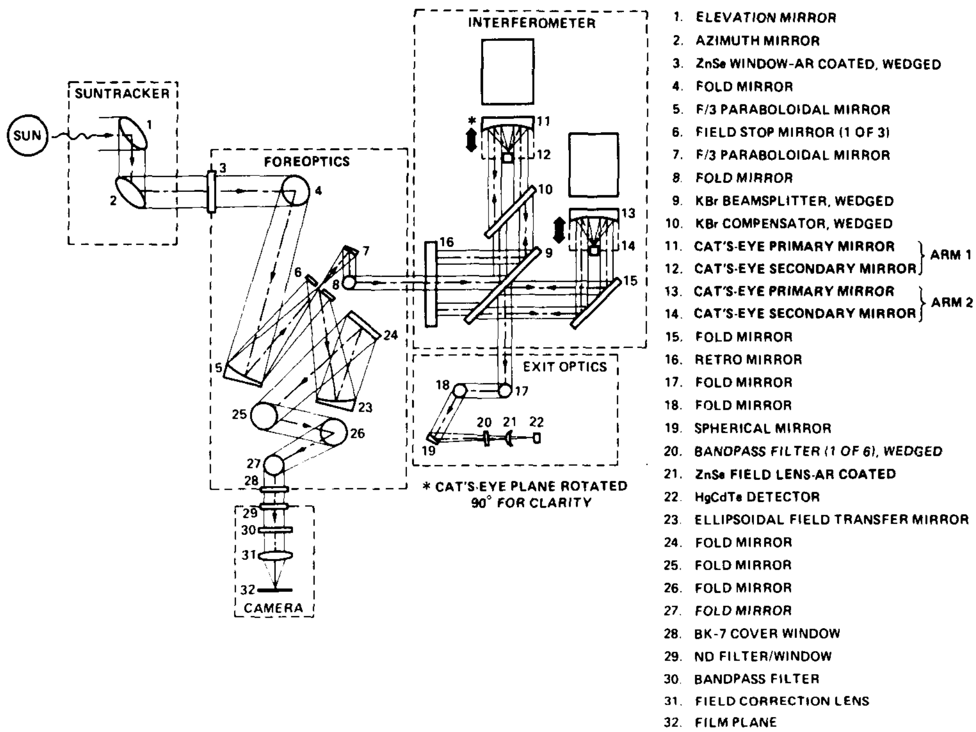

Fig. 4. Optical diagram of the foreoptics and interferometer of the ATMOS sensor.

levels: (1) an outer control that uses a phase-locked loop to convert laser feedback to an error signal and provides the precise velocity control; and (2) two inner control loops, one for each slide, that use moving coil tachometers for velocity feedback. The function of the inner loops is to force both slides to operate at approximately the same velocity. As each slide reaches the end of its travel, control is switched to position feedback with the loop closed around Linear Variable Differential Transformer (LVDT) position sensors; the return scan is initiated after both sliding assemblies are brought to a halt in their hold positions. To maximize the duty cycle, scan control is provided in both directions with turnaround times of 150 ms at each end.

The output from the interferometer passes through one of the six selectable bandpass filters and is focused by an AR-coated ZnSe lens onto a photoconductive HgCdTe detector, where a pupil image is formed. The detector is a single element, 27 mils on a side; the size of the chip was chosen on the basis of both sensitivity and linearity requirements under high-signal flux conditions. It is AR coated to improve quantum efficiency and uses a constant bias voltage to improve linearity. The element is packaged in a sealed glass vacuum dewar and cooled to 77 K using a split-Stirling-cycle mechanical cooler with a 1.6-watt cooling capacity.

3. Electronics Description

The output from the detector is transferred to the SHSS, where it is amplified, filtered, and digitized for insertion into the DHSS. The SHSS, shown schematically in Fig. 6, has been designed to preserve source-noise-limited performance while accommodating an expected dynamic range of 18 bits with minimum phase and amplitude distortion. The 18-bit-dynamic-range, high-data-rate operation is obtained through the use of two 12-bit parallel data channels offset in gain by 5, 6, or 7 bits, selectable by command. Both outputs are included in the PCM data stream. During ground processing, valid data from each channel is interleaved to reconstruct an effective 18-bit signal that preserves peak signal precision and maintains source-noise-limited performance at high-spectral resolution. Sampling of the analog interferogram in both channels is based on delayed reference laser fringe sampling at every second (395 kHz) or third (263 kHz) laser fringe, selectable by command. Electronic distortion has been minimized through proper delay of the sampling waveform as well as through use of multipole compensated Butterworth filters for noise bandlimiting.

The remaining elements of the ATMOS electronics are shown in Fig. 7. The DHSS accepts the digitized high- and

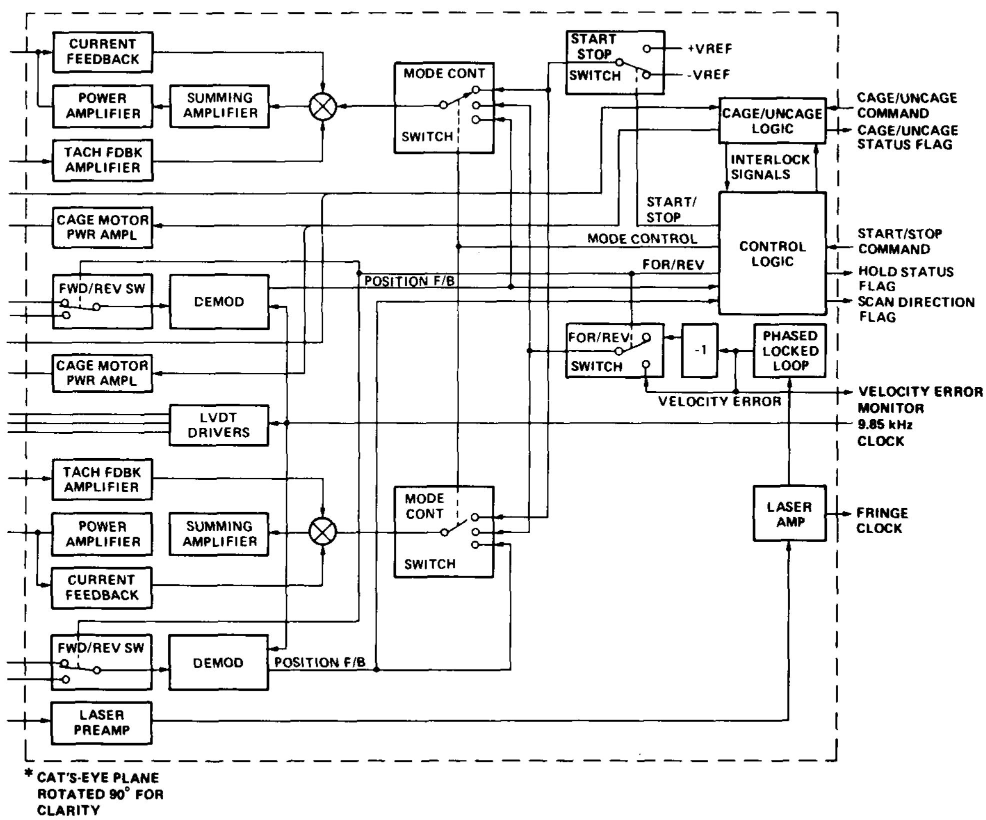

Fig. 5. Schematic of the ATMOS servo system.

low-gain interferometric data to be buffered and formatted into a Shuttle-compatible Non-Return to Zero-Logic (NRZ-L) serial 15.76-Mbit/s PCM data stream. The formatting section is a hard-wired design with formatting accomplished by a digital multiplexer. The high-rate data format includes the engineering and housekeeping data and both time and optical path position references. Also shown in the block diagram are the main elements of the EDHSS and CCISS. A common feature of these subsystems is a Motorola MC6802 microprocessor that formats the system engineering and housekeeping data as well as decoding and implementing the instrument commands received through the Shuttle interface. In addition to the high-rate PCM data channel, the ATMOS instrument provides a 1.28-kbit/s low-rate PCM output containing engineering and housekeeping data only.

D. Instrument Support Equipment

The ATMOS instrument requires dedicated ground support equipment for operation and testing in the laboratory, status monitoring on orbit, and recording of high-rate science data during both ground and flight operations. The ground support equipment is divided into two primary elements: the Bench Checkout Equipment (BCE) and the Ground Support Subsystem (GSS). The BCE consists of a single rack of equipment that directly supports the instrument by providing it with power and a command interface, duplicating the services that the Spacelab provides during a mission. The rack provides a +28 Vdc power supply for the instrument's electronics and a 400-Hz, three-phase, 115 Vac motor generator to power the instrument's cryogenic cooler compressor. The command interface consists of an Intermetrics Spacelab Experiment Interface Device (SEID) that emulates the functions and signal characteristics of a Spacelab Remote Acquisition Unit (RAU). It provides two discrete pulse lines to turn on and turn off the main dc power system in ATMOS, a serial line that provides Greenwich Mean Time (GMT) code signals and instrument subsystem commands, and a clock synchronization signal that updates the GMT every 0.25 s. The SEID is operated through a terminal or a microcomputer via an RS-232C serial interface. Most of the ground operations commanding is done through a BASIC program command shell running in an Epson HX-20 lap-top microcomputer.

The GSS consists of three major groups of hardware. The first is the data-receiving interface, which is connected either to the ATMOS instrument during ground testing or to the data distribution interfaces at Kennedy Space Center (KSC) and

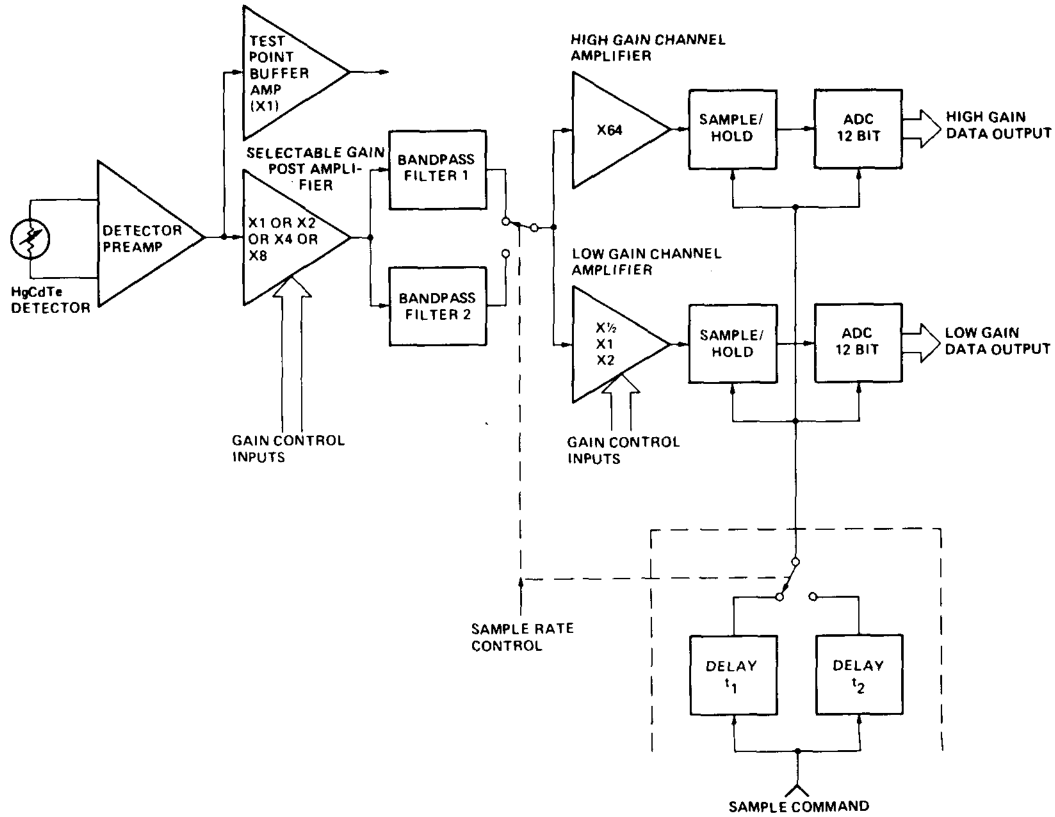

Fig. 6. Schematic of the ATMOS signal-handling subsystem.

Johnson Space Center (JSC). Both the 15.76-Mbit/s high-rate science data lines and the 1.28-kbit/s low-rate engineering data lines, each consisting of a PCM data line and a clock line, are connected to the GSS PCM interface unit. This box conditions the incoming signals and routes them to the proper destination within the GSS. Incoming low-rate data is sent to a DCS 4003A card programmable PCM decommutator, where the data structure is verified and the data format is serial-to-parallel converted. The low-rate data is passed on to the second group of hardware, a Digital Equipment PDP 11/34A minicomputer, in which the engineering data is converted from data numbers to engineering units. The results are displayed on a Tektronics 4010 terminal in the form of four pages of engineering parameters comprising instrument subsystem status, filter and FOV positions, suntracker pointing direction, and subsystem temperatures, pressures, and voltages. Hard copies of each engineering display page can be made on a Tektronics 4361 hard-copy unit.

E. Ground Testing

The first interferograms generated with the ATMOS instrument using the Sun as the source were recorded by HEOC in October 1982. In order to evaluate the instrument's performance on the Sun, interferograms were generated using all possible combinations of the ATMOS filters and aperture sizes. At the time the tests were conducted, a suitable flight detector was not yet available for the instrument, and it was thus necessary to record the interferograms using the engineering detector. To compensate for the relative insensitivity of this detector, several spectra of each type were averaged to increase the signal-to-noise ratio to one more representative of that expected from the flight unit. Some excerpts from the resultant spectra are shown in Figs. 8 through 13.

These spectra, which were processed in the ATMOS Data Analysis Facility (DAF), validated the instrument's performance and signified its readiness to enter the environmental test program. This program was initiated in November 1982 and included vibrational, thermal vacuum, and Electromagnetic Interference (EMI)/Electromagnetic Compatibility (EMC) testing.

In the course of the vibrational testing, the instrument experienced a slippage of the cat's-eye adjustment; since this slippage did not invalidate further testing, the problem was recorded and testing was continued. During the low-temperature thermal-vacuum test sequence, an electronic failure occurred

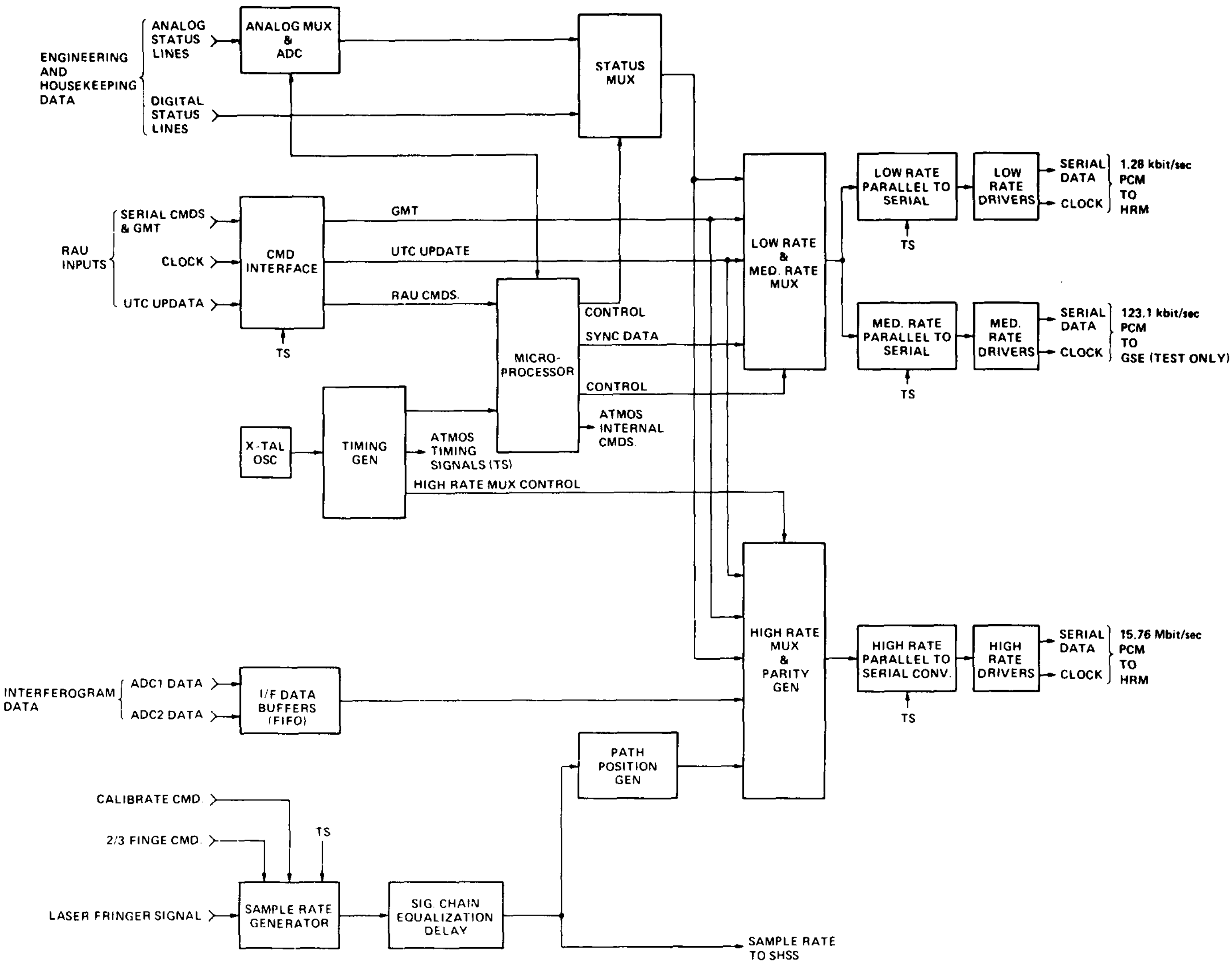

Fig. 7. Schematic of the remaining elements of the instrument electronics.

on the data formatter board that was subsequently corrected by circuit modifications. Excessive temperature, experienced at space vacuum, was traced to an indium metal thermal joint between the Secondary Electronics Unit (SEU) plate and the compressor assembly. This joint was modified and repaired by lapping and by the use of a thermal joint compound. Finally, a failure encountered during the conducted-susceptibility part of the EMI/EMC testing was traced to a power supply; this problem was also flagged for later correction.

A Preshipment Review and a Predelivery Review were held in December 1982 and January 1983 to assess the status of the instrument and to plan the logistics for the shipment to JPL. In both cases, the boards recommended that Honeywell proceed with the shipment.

F. JPL Preflight Activities

In February 1983 the instrument, the GSS, the BCE, and miscellaneous spare parts were shipped via air freight to JPL. Upon arrival, the instrument was installed in its own clean room in the Spacecraft Assembly Facility at JPL, and a complete inspection was conducted that revealed no damage to the equipment during the shipment. As part of this receiving inspection, a System/Subsystem Test (SST) was run that verified the proper operation of all ATMOS subsystems.

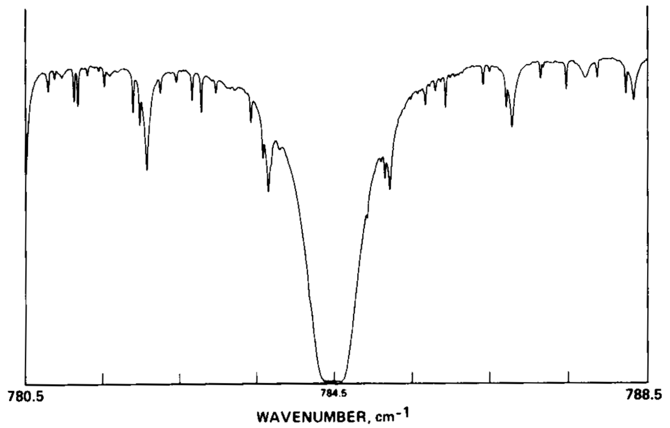

Fig. 8. Spectral excerpt from the first ATMOS ground-based spectra showing a large water line surrounded by smaller features of ozone and carbon dioxide.

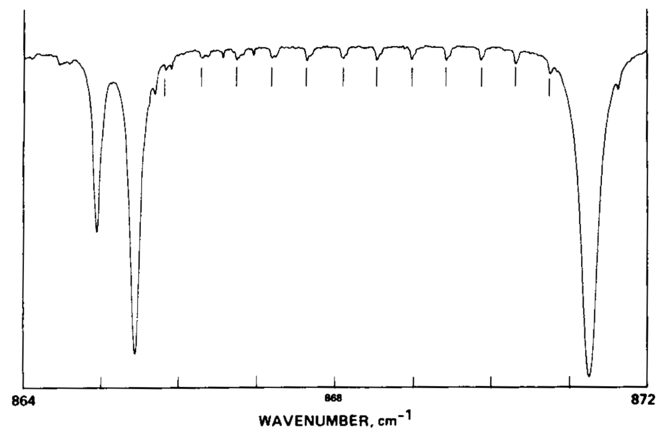

Fig. 9. Spectra excerpt from an ATMOS ground-based spectrum showing the atmospheric features of nitric acid (marked by vertical bars).

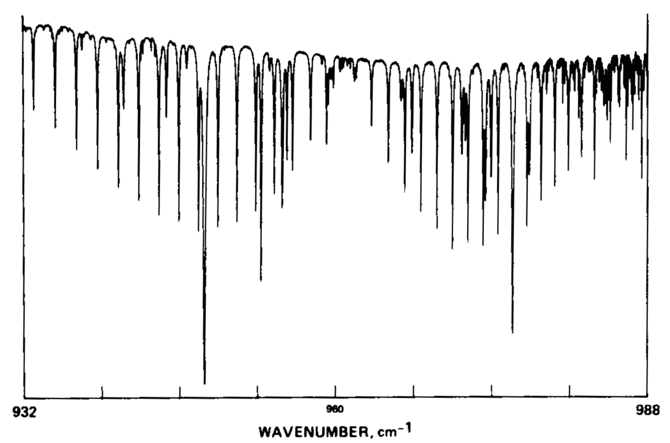

Fig. 10. A weak hot band of carbon dioxide taken from the first ATMOS ground-based spectra. The three largest features are due to water vapor.

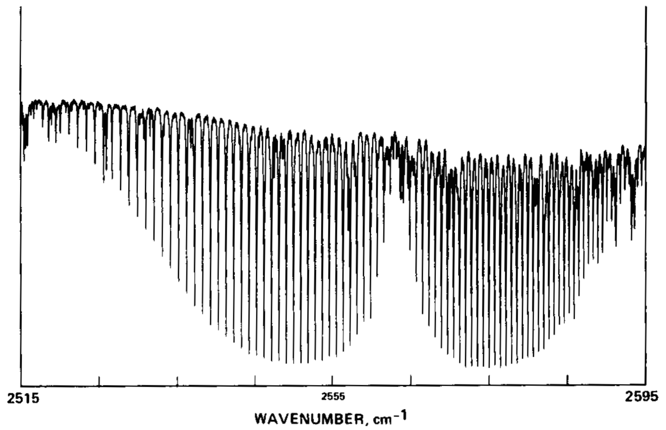

Fig. 11. A ground-based spectral view of one of the fundamental bands of nitrous oxide centered at ~2560 wavenumbers.

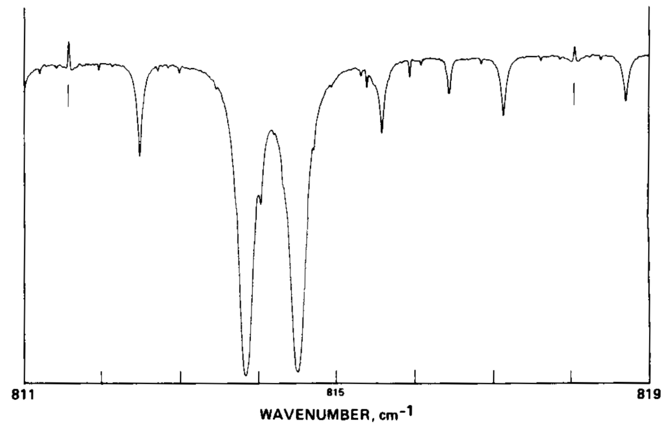

Fig. 12. The features marked by vertical bars in this figure are emission lines from the photosphere of the Sun. They have been characterized by some solar physicists as lines from highly ionized magnesium.

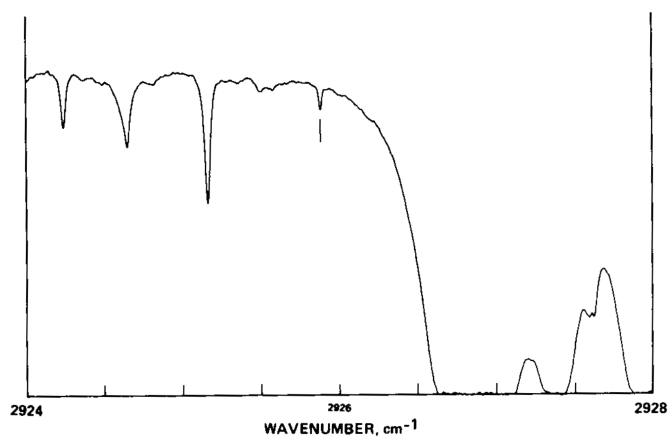

Fig. 13. The vertical bar in this figure marks the R1 line of the 1–0 transition of HCl. HCl was first detected in the atmosphere both from the ground and from an airborne platform by an early precursor of the ATMOS instrument.

The power supply that had failed during the EMC tests was removed in March 1983, returned to Honeywell for modification, and retested to confirm that the problem had been corrected. Upon reinstallation of the power supply, the complete SST was rerun to verify all system components.

The first flight detector was delivered to JPL and installed in August 1983. Preparations were then begun for the first solar tests of the complete flight system. During these preparations, a long-standing cooler/compressor instability problem recurred, and the decision was made to do a complete investigation into the cause. A mass spectrometer analysis of the cooler gas was made that revealed a large percentage of N_2, H_2O, Ar, and CO_2 contamination in the presumedly pure Helium. All of these gases are condensable at the 77 K operating temperature of the cooler and were suspected to be the source of the instability and failures experienced with the cooler throughout the instrument development period. It was further suspected that a Teflon-lined charging hose was responsible for the contamination. The problem was eliminated through the adoption of a rigorous purging-charging procedure using high-purity Helium gas through a newly constructed stainless steel charging manifold. All subsequent operations with the cooler, including the on-orbit performance during the SL-3 mission, have been very stable and reliable. During the cooler rework, loose parts in the form of thin metal shims were also discovered and removed from the instrument.

As previously mentioned, the instrument was delivered with the cat's-eye travel incorrectly positioned as a result of slippage during vibration testing. The cat's-eyes were adjusted at JPL to provide the ±50 cm OPD required to produce a symmetric, two-sided interferogram, and new clamps were installed on the cat's-eye assemblies to provide positive locking of these adjustable mechanisms. A subsequent solar test revealed an unknown instability in the interferometer slide operation at the FOVs of 2 mr and 4 mr. This was traced to stray light in the interferometer cavity that flooded the laser detector and thus caused nonlinearity in the servo system, leading the cat's-eye slides to run out of control. Through testing and analysis, it was determined that the addition of a polarizing filter over the laser would eliminate the stray light causing these nonlinearities. Solar tests made subsequent to these modifications verified that the instrument performance and the detector signal-to-noise characteristics met the requirements for the ATMOS investigation.

During the fall of 1983, a failure in the environmental control system in the ATMOS clean room subjected the KBr beamsplitter and compensator to high humidity, clouding them and destroying their optical properties. To recover from this failure, a new matched beamsplitter and compensator pair were fabricated, coated, and mounted in their cells, and the interferometer was completely realigned. As a consequence of these modifications, the overall instrument performance was somewhat improved over the as-delivered configuration. This was evidenced in a final set of solar measurements made for the purpose of extrapolating the instrument gain settings as a function of filter and aperture to their on-orbit values.

Because of the extensive modifications to the optomechanical components, a three-axis flight-level workmanship vibration test was performed and completed in November 1983; no problems or failures were experienced during this test. In the same time frame, the Project conducted a Preshipment Review with the ATMOS Review Board, and delivery of the instrument to KSC for integration into the SL-3 payload was authorized. In early January 1984 the instrument and its ancillary support equipment were shipped to KSC in preparation for the SL-3 integration activities.

Section III
Spacelab 3 Integration

A. KSC Delivery and Off-Line Testing

The ATMOS flight instrument and GSE arrived at the KSC Operations & Checkout (O&C) building loading dock on January 6, 1984. The flight hardware was received, inspected, and moved to the off-line testing area. Prior to being moved, the standard NASA/European Space Agency (ESA) cold plate, located on the underside of the ATMOS substructure, was cleaned by KSC technicians and certified by KSC Quality Assurance. The instrument, GSS, and BCE were then set up in an off-line room, and tests were run to verify that no damage had occurred during the shipment to the Cape. As a part of the tests, high-rate data was recorded using a 950 K blackbody as an energy source and sent back to JPL for computer analysis.

After the off-line test, the status of the instrument and its documentation were reviewed by Marshall Space Flight Center (MSFC) and KSC integration and safety personnel, following which the ATMOS instrument and its supporting flight hardware were turned over to KSC for integration into the SL-3 payload. The instrument, Multi-Layered Insulation (MLI) blankets, MLI frame, thermal isolators, mounting hardware kits, and solar simulator as well as all associated lifting fixtures were placed in bonded stores to await Level IV integration. The GSS was moved to an on-line Users' Room on the fourth floor, and the BCE was moved to a staging area near the Level IV assembly stands on the main floor of the O&C building.

B. Level IV Integration

ATMOS was mounted on the MSFC-supplied Mission-Peculiar Experiment Support Structure (MPESS) in late January 1984. The MPESS is a large, open-truss structure that spans the width of the orbiter payload bay at the level of the payload bay door hinge line. It is attached to this hinge line and to the orbiter keel. A specially designed three-point kinematic support fixture was mounted to the top of the MPESS, and four epoxy fiberglass thermal isolators were bolted to the support fixture with 16 hardened 3/8-in. X 3-in. bolts using special, thick washers. Locking nuts made of special hardened alloys and additional thick washers were then used to secure the instrument to the thermal isolators.

1. Level IV Functional Test

When initially turned on for Level IV testing, the ATMOS instrument failed to acknowledge any of the serial commands that were sent to it. The problem was traced to an incorrectly wired serial command line and was remedied by the switching of the signal and return lines in the Spacelab cable connector by KSC technicians. Every subsystem was then thoroughly exercised with command sequences that included a typical set of commands to be executed during the actual Spacelab mission. No further problems were experienced during the remaining functional tests.

2. Level IV Mission Sequence Test

The Level IV Mission Sequence Test was conducted in late March 1984. The test was conducted with real flight hardware and simulated flight software and was designed to uncover possible interferences between experiments and any problems with the mission plan, including the Master Timeline (MTL). This test simulated segments of the week-long mission from payload activation through deactivation and utilized slices of the SL-3 timeline that exercised all the experiments on board. The timeline slices took the instrument through several of the mission observation sequences, including an emergency shutdown procedure. ATMOS performed nominally throughout Level IV, and no interference between the interferometer and the other experiments was detected.

C. Level III/II Mission Sequence Test

At Level III/II, all the SL-3 experiments were integrated into the actual flight hardware, and a second mission sequence test was conducted. The ATMOS instrument again performed nominally during these tests despite a problem with the GSS that required the services of the design engineers from HEOC.

D. End-to-End Test

The SL-3 payload was moved to the Orbiter Processing Facility (OPF) in March 1985, and the entire assembly was integrated into the Orbiter Challenger. During this time the ATMOS GSS was shipped to JSC in Houston and installed in a Users' Room in the Payload Operations Control Center (POCC).

The last test of the ATMOS instrument prior to its SL-3 flight was a complete end-to-end test of the entire NASA/Spacelab data network. This test was conducted in early April 1985, just four weeks prior to the scheduled launch. The test involved powering up the Orbiter Challenger and the entire SL-3 payload and operating the experiments from the POCC facility at JSC. Commands and data were sent between the POCC and the experiments through a data link that involved transmissions through the Spacelab interfaces to the Challenger's Ku-band antenna, the Tracking and Data Relay Satellite System (TDRSS) satellite, the White Sands ground station, a domestic communications satellite, and the command and data-handling systems of JSC/POCC, MSFC, and other NASA facilities. All the SL-3 experiments that were tested during this period performed nominally.

Section IV
Mission Planning

A. Background

The ATMOS Investigation was originally proposed for and accepted as a part of the Spacelab 1 (SL-1) mission. Initial design efforts were directed at locating the interferometer in the Scientific Air Lock (SAL), which was a part of that mission with the electronics in a nearby rack. Early in the program, it was recognized that a dependence on the SAL could severely restrict the number of reflight opportunities for ATMOS, and since the experiment was to involve multiple reflights over a period of several years, the design concept was altered to that of an integral instrument that could be mounted on the Spacelab pallet. By that time, however, the SL-1 pallet was full, and as a consequence the first ATMOS flight was remanifested onto SL-3.

As a result of the reassignment to SL-3 and the numerous slips in the launch date for that flight, mission planning for the investigation became a very dynamic activity. Since the experimental goals are dependent on the season and the latitude coverage achievable, each launch slip required a complete replanning of the measurement strategy for ATMOS. Fortunately, ATMOS was essentially the only experiment on SL-3 that was sensitive to latitude versus time of day and was thus allowed to select the time of launch, which in turn determined the latitudes of the sunrise and sunset occultations throughout the mission. This is illustrated in the "bow tie" plot in Fig. 14, which shows the actual launch time chosen for SL-3 and the resultant latitudes for the sunrises and sunsets.

The launch time of 1700 hours Eastern Daylight Time (EDT) shown in Fig. 14 was chosen primarily to obtain as many occultations as possible at northern midlatitudes. This was considered to be the overriding priority for the first mission, since it would allow a critical comparison to be made between the ATMOS measurements and those obtained with other instruments, the bulk of which had been made in these regions. Coverage was planned such that as many latitudes as possible were sampled in all four of the primary filter regions. While the sunrise measurements at somewhat higher southern latitudes were of relatively low priority, they still provided contrasting seasonal and hemispheric comparisons.

B. Master Timeline

The normal strategy for planning the ATMOS mission was to study the bow tie plot provided by MSFC for the launch opportunity, select the launch time appropriate to the experiment objectives, and request a specific number of measurement periods based on the objectives to be met. The SL-3

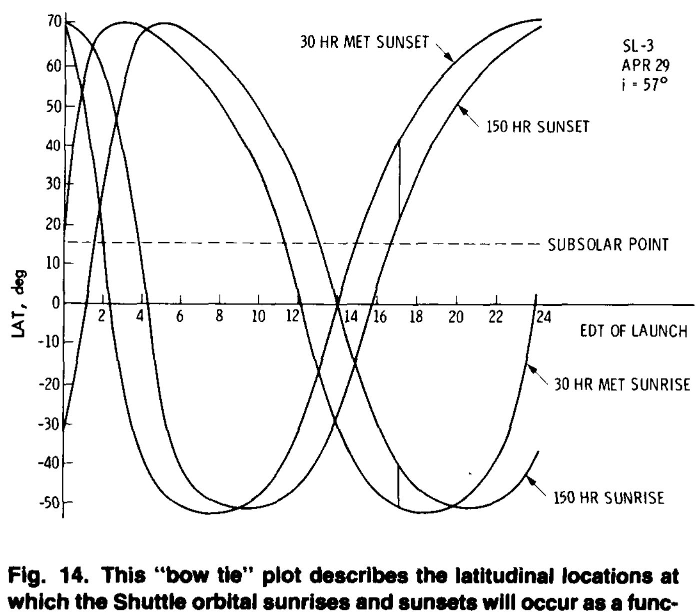

Fig. 14. This "bow tie" plot describes the latitudinal locations at which the Shuttle orbital sunrises and sunsets will occur as a function of the launch time for a given day (April 29). The vertical bars at 1700 hours represent the actual time chosen by ATMOS, primarily to provide good coverage of northern midlatitudes.

Mission Manager then factored this request into the overall requirements for resources for all the SL-3 experiments and attempted to meet as many of these needs as possible. On the basis of the resources thus allocated, the ATMOS team developed an experiment timeline to be run by the Spacelab MTL, which controlled all of the operations of the ATMOS instrument from the initial turn-on to the final shutdown. The MTL monitored the main orbiter clock in both GMT and Mission Elapsed Time (MET). At preprogrammed times, the MTL either executed direct commands (to turn on an experiment's power, for example) or branched to time-driven subroutines known as Subordinate Timelines (STLs). In the case of ATMOS, each sunrise-sunset occultation or calibration had its own unique set of STLs. Each STL comprised instrument commands that would power up subsystems; select the proper optical bandpass filter, FOV, and gain; preposition the suntracker to the predicted Sun position; acquire the Sun; capture data; and then power down the instrument subsystems. By way of illustration, Table II-1 in Appendix II shows a segment of the experiment timeline covering a single occultation. Table II-2 is a summary of all the planned occultations for the ATMOS investigation on SL-3 as a function of type of measurement, time of measurement, and optical filter used. As Table II-2 indicates, there were three primary functional objectives for ATMOS: atmospheric occultations, full Sun observations with no intervening atmosphere, and measurements of the dark sky with no source present. ATMOS was the most intensive user of the MTL during the SL-3 mission.

Section V
The Spacelab 3 Flight

A. Mission Operations

The SL-3 mission operations were conducted by JSC's Mission Control Center (MCC), the MSFC POCC cadre, and experiment teams representing each investigation. The ATMOS POCC user area contained the ATMOS GSS, three display terminals, three voice consoles, and a Tektronix 4025 Graphics terminal connected via a 9600-baud line to the DAF at JPL. The ATMOS team consisted of two three-person crews working in 12-hour shifts. These crews recorded incoming ATMOS data on the Ampex recorder, monitored the status of the experiment via custom-designed graphic and tabular displays of the engineering data on the POCC terminals, and interacted with the MSFC cadre on the voice consoles. As the mission progressed, the Ampex data was reformatted into Computer Compatible Tapes (CCTs) and shipped to JPL for processing. The quality of this data was then evaluated with the aid of the 4025 terminal in the POCC. Three other team members, including the Principal Investigator, worked asynchronously in the evaluation of the processed data, in the Science Operations Working Group (SOWG) and daily replanning meetings, and in the shipment of data to JPL as it was received.

B. ATMOS Flight Operations

The SL-3 mission (Space Transportation System [STS] flight 51B) was launched aboard the Space Shuttle Challenger at 21:00:30 hrs GMT on April 29, 1985; payload activation was at Launch + 4 hours (4 hrs MET). The ATMOS instrument was commanded on and into its standby mode at 6 hrs 24 min MET and began the transmission of low-rate data.

It was immediately apparent in the low-rate stream that a potential problem was developing with the interferometer. The pressure in the reference laser housing, nominally 14.7 psi, was down to 8.9 psi and dropping, indicating the presence of a leak in the system. The implication of this leak was that a high-voltage breakdown in the laser starting system would eventually occur, thus terminating the experiment. This information was communicated to the Mission Manager, who immediately initiated a replanning effort to move forward as many ATMOS observations as possible in the MTL. That the ATMOS instrument obtained sufficient data to ensure the success of the experiment is a tribute to the Mission Manager, the SOWG, and MSFC cadre personnel, who successfully accomplished this task without compromising the data return of the other investigations. It also demonstrated the effectiveness of the replanning procedures that had been established to deal with unplanned contingencies.

The first ATMOS observation was a gain calibration to establish the proper common- and low-gain settings for each filter position. This was done by viewing the nonocculted Sun and recording data through each of the six filters at three different gain settings: calculated nominal, 2 X nominal, and 1/2 nominal. During this observation, the zero-path difference voltage was monitored with the POCC terminal graphical displays, and the calculated gain settings were found to be correct in all cases, precluding any changes in the ATMOS STLs.

The SL-3 launch was delayed by 30 seconds, which resulted in a timing problem for the first two ATMOS occultations. Following these, the MTL was updated to correct for the delay, and all subsequent observations proceeded nominally. However, the laser housing pressure continued to drop, and at the beginning of the 25th occultation the laser failed to respond to the on command. A number of subsequent attempts to start the laser by direct ground command were also unsuccessful, and the instrument was finally turned off at 3 days 17 hrs 31 min MET.

Before it was turned off, the ATMOS experiment recorded 19 complete atmospheric occultations, four solar calibrations, and one dark sky calibration. The geographic locations of the measurements are shown in Table 2. Over 200 CCTs were generated from the data set, ultimately producing 1474 solar spectra and 1192 atmospheric spectra. A summary of the returned data is shown in Table 3.

Other than the loss of the laser housing pressurization that resulted in the premature termination of the data acquisition, the instrument's performance during the SL-3 mission operations was nominal or better in all respects. In particular, the slide velocity stability was better than that achieved during testing on the ground with a peak-to-peak variation of 0.15%. Temperatures were well within the 15 C° to 30 C° fluid cooling loop range, and the detector cool-down time of 7 minutes was exactly the same on orbit as on the ground. The suntracker pointing stability was better than 0.1 mr in both azimuth and elevation, and the laser's frequency stability and power output were unaffected until the final loss of housing pressure.

The bit-error rate of the data during the period of operation, averaged approximately 5×10^{-7} over the entire data set. However, errors came in bursts of several thousand bits, as established by checking the instrument parity, rendering an occasional interferogram unusable but having little impact on the mission; the vast majority of interferograms were received error free. Less than 2% of the spectra were lost because of uncorrectable bit errors. This type of error performance is evidently characteristic of the TDRSS satellite link and is quite acceptable for the downlinking of interferometric data.

Table 2. A summary of the occultations by filter and geographical location returned by the SL-3 flight.

Start Time (MET)	OCC Type	OPT Fil	Start Lat	Start LON (E)
00/07:13	SR01	3	–50.10	118.25
00/08:08	SS01	1	36.87	277.60
00/18:52	SS02	1	36.18	117.31
00/19:27	SR02	3	–49.12	294.55
00/21:55	SS03	2	34.53	70.68
01/00:55	SS04	4	35.82	25.69
01/01:34	SR03	6	–49.10	203.09
01/02:28	SS05	1	34.80	2.26
01/07:01	SS06	3	32.90	292.66
01/08:33	SS07	2	33.65	270.20
01/10:05	SS08	1	33.73	247.39
01/15:18	SR04	4	–47.28	355.90
01/16:49	SR05	2	–47.80	333.43
01/18:21	SR06	1	–47.15	310.09
01/19:53	SR07	5	–46.97	287.07
02/01:22	SS09	3	29.95	16.84
02/02:53	SS10	4	30.28	354.13
02/04:25	SS11	3	29.00	330.65
02/05:51	SS12	2	28.65	307.61
02/07:27	SS13	3	29.65	285.23

Table 3. A summary of the yields from the data reduction processing of the ATMOS data.

Occultation No.	Filter No.	# High Sun Spectra	# Atmospheric Spectra	Total # Spectra	Height of Highest Telluric Spectrum
CAL1	All		not processed		
SR01	3	28	10	38	138 km
CAL2	All		not processed		
SS01	1	110	44	154	139 km
SS02	1	92	58	150	137 km
SR02	3	54	68	132	132 km
SS03	2	76	70	146	139 km
SS04	4	58	62	120	141 km
SR03	6		not processed		
SS05	1	54	58	112	137 km
SS06	3	32	68	100	138 km
CS1	1		not processed		
SS07	2	54	68	122	140 km
SS08	1	66	76	142	136 km
SR04	4	82	60	142	139 km
SR05	2	86	78	164	139 km
SUN1	6	148	--	148	
SR06	1	88	64	152	138 km
SR07	5	50	62	112	138 km
SS09	3	60	68	128	138 km
SS10	4	52	72	124	140 km
SS11	3	56	64	120	137 km
SUN2	4	110	--	110	
SS12	2	48	76	124	139 km
SS13	3	70	66	136	132 km

Section VI
ATMOS Data Reduction and Analysis

A. Data Analysis Facility

The ATMOS DAF is centered around a Prime model 9955 super-minicomputer capable of 5.5 million instructions per second. Attached to the Core Processing Unit (CPU) are peripherals that are typical of most installations, including two 800/1600/6250 Bits per Inch (BPI) magnetic tape drives and four moving-head disk drives with a total storage capacity of 1500 Mbytes. The peripherals that make the ATMOS system unique are three Floating Point Systems model 5205 array processors, each capable of 12 million floating point operations per second. An external Shared Access Memory (SAM) from Texas Memory Systems, consisting of 16 Mbytes of Random Access Memory (RAM), is attached via high-speed (5 Mbytes/s) interfaces to each array processor. The acquisition and utilization of this system solved the computation time problem associated with the voluminous mathematical operations inherent in the reduction and analysis of interferometric data sets as large as those produced by the ATMOS instrument.

B. Data Processing Software

There were two principal tasks involved in reducing the SL-3 data: first, data calibration, which involved stripping the infrared words and other information from the recorded telemetry stream, error checking, and reformatting; and second, the Fourier transformation of the interferogram to produce a spectrum. The program that accomplishes the first task is called the Interferogram Processing Program (IPP), while the second has been named the Fourier Transform Program (FTP). The nominal time to process each raw interferogram through both programs and to produce a finished spectrum was about four and one-half minutes.

1. Interferogram Processing Program (IPP)

The telemetry rate of the ATMOS instrument is 15.76 Mbits/s. The maximum sampling rate of the interferogram, on the other hand, is 400,000 32-bit words (or 12.8 Mbits) per second. This means that, periodically, the data subsystem must insert a "stuff" word into the data stream in order to maintain the required data rate. The presence of these stuff words has proved useful in that the additional and redundant information available in the ATMOS data stream can be used to enhance error correction.

The ATMOS data format is built around standard telemetry principles. The data is arranged in blocks known as major telemetry frames, each consisting of 96 shorter records known as minor telemetry frames. An ATMOS minor frame consists of a synchronization word, an engineering or "housekeeping" word, 125 science words, and a final parity word, making the minor frame length 128 32-bit words. Each 32-bit sample has a longitudinal parity bit in it, which is turned on or off as necessary to ensure that the sum of all set bits is odd. The vertical parity bit in each is also turned on or off such that the sum of all set bits in a vertical column (constant bit position) is also odd. Therefore, when a parity error occurs, it is possible to both detect and correct a single parity error in a minor frame. In fact, the redundancy in the ATMOS data stream makes it possible to correct multiple parity errors in a minor telemetry frame.

Each ATMOS data sample consists of a 12-bit low-gain channel value, a 12-bit high-gain channel value, a 5-bit path-position value, individual bits for data validity (indicating whether or not the slides are in the turnaround mode), "stuff" status (whether the word is a legitimate sample or a stuff

PRECEDING PAGE BLANK NOT FILMED

PAGE 24 INTENTIONALLY BLANK

word), and a parity bit. In processing an ATMOS scan, the IPP first reads a block of data from magnetic tape into the computer memory. It is then transferred to an array processor, where single-bit parity correction is attempted if necessary. If not successful, control returns to the Prime computer, where multiple-bit parity correction is attempted, and the corrected record is retransferred to the array processor. Next, the low-gain and high-gain sample values are stripped from the array, stuff words are identified and eliminated, and the resulting arrays of low-gain and high-gain samples are written to the SAM memory system. This process is continued until the end of the scan is signaled by the majority of the data valid bits in a minor frame indicating that the data is no longer valid. As the blocks of data are written to the SAM, the program monitors the peak value of the low-gain channel, which indicates where in the scan the white-light fringe occurs and calculates the dc level of each channel. The gain ratio between the channels and the dc levels of each channel are all that is needed to create a single-channel interferogram from the two channels. This interferogram is written back to the Prime disk, labeled with the GMT to the nearest second occurring prior to reaching the zero OPD fringe.

2. Fourier Transform Program (FTP)

The FTP performs two principal tasks: the nonlinear phase correction of the interferogram and a complex-to-complex in-place Fourier transform. To perform the phase correction, a short double-sided transform of the interferogram is done, the phase spectrum and then its conjugate are calculated, and the inverse Fourier transform of the conjugate phase spectrum results in the interferogram phase-correcting function. This function is then convolved with the interferogram to produce one that is symmetric in the near vicinity of the white-light fringe; the amplitudes in the wings of the interferogram are not corrected.

The Fourier transform algorithm used involves a number of matrix transposes, and since one of the salient features of the SAM memory system is that it can perform a matrix transpose "on the fly" with no overhead, it can be seen that this algorithm is ideally suited to the DAF hardware configuration. On the ATMOS computer system, the matrix transposes are not actually performed. Instead, when the elements of a particular row of the original matrix are needed in the memory of the array processor, a scatter read of the SAM memory is performed. After the discrete transform is complete, a scatter write to SAM memory is performed, and the elements return to their original positions. In the second phase, the SAM memory is read and written sequentially by columns. In the final phase, when the ATMOS spectrum is written out to the disk system of the computer, a scatter read of the SAM memory is again performed for each block.

C. Temperature-Pressure Retrievals

In order to determine the vertical mixing ratio profiles of the minor and trace constituents from the ATMOS data, it is first necessary to determine the temperature and pressure profile over the relevant region of the atmosphere. Spectral features are present in the ATMOS data that can be used to extract these quantities from a number of the individual occultations. Lines from several ground-state transition bands of CO_2 can be used to determine pressure and temperature over altitudes from 20 km to approximately 70 km, and, by virtue of their insensitivity to temperature, the S8 and S10 lines from the N_2 1–0 quadrupole band, which have lower state energies on the order of 200 cm^{-1}, can also be used to retrieve line of sight column density from 20 to 35 km. Since tangent ray paths in this region correspond to airmass values between approximately 10 and 1, the N_2 lines can be carefully "calibrated" by reference to spectral scans made by the instrument observing the Sun from the ground at equivalent airmasses. Temperature is determined from moderately absorbing temperature-sensitive high-J CO_2 lines. Both the high-J CO_2 lines and the N_2 quadrupole lines can be seen in the spectral excerpts in Fig. 15. Retrieval below 20 km is difficult because of interfering absorptions from other gases, but this region is of lesser importance to the objectives of the experiment. Above 80 km, certain assumptions made in the analysis break down; the CO_2 volume mixing ratio falls off due to photolysis, and the atmosphere is no longer in hydrostatic equilibrium.

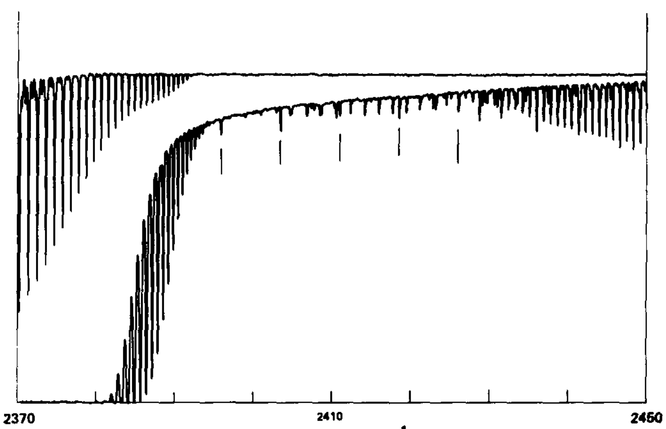

Fig. 15. Two spectral excerpts from the temperature-sensitive high-J region of the $\nu 3$ band of CO_2 and the pressure-induced absorption region for N_2 (the depression in the continuum in the lower trace is primarily due to the latter dipole absorption). The features marked by vertical lines are the temperature-insensitive N_2 quadrupole lines used for density retrievals (identified from left to right as the S7 through S11 lines). Note that in the upper trace no absorption by N_2 can be seen, even though N_2 is still the dominant gas in the region. This demonstrates the weak nature of both the dipole and quadrupole absorptions.

These effects can actually be seen in spectra above a tangent altitude of approximately 70 km, which thus represents the upper limit for pressure and temperature retrievals using this method.

Four separate groups of ATMOS coinvestigators developed independent algorithms to retrieve temperature and pressure based on the general methods mentioned above. Three of the groups measured and utilized the equivalent width of the spectral lines under study, while one used nonlinear least-squares spectral curve fitting. Of the three equivalent width method groups, two retrieved temperature and pressure at all levels simultaneously. The other two groups analyzed the spectra with an iterative "onion-peeling" approach. The establishment of four different working methods allowed for an intercomparison of results. The standard deviation among the groups for an individual Northern Hemisphere occultation was on the order of 2% for temperature and 5% for pressure, and thus an average profile was created from the four group's retrievals for each Northern Hemisphere occultation analyzed. A grand zonal-mean profile was ultimately created from these averages, and this physical model was adopted for all the Northern Hemisphere analyses. For the Southern Hemisphere, the disparity among the groups' retrievals was larger than for the north, but an average of the four groups' models for sunrise number 2 (recorded through filter 3) was finally selected as the most representative physical model for all the Southern Hemisphere measurements.

D. Science Analysis Software

The approach adopted for deriving the profiles of concentration from the data was to preselect very narrow wavelength regions in the spectra that contain analyzable features of each gas of interest and to manipulate these "microwindows" rather than the huge spectral sets themselves. To give an indication of the quality of the data and to illustrate the remarkable power of the Fourier transform technique when used in this way, the top trace in Fig. 16 shows a segment of about 500 cm^{-1} from one of the filter 2 observations. The succeeding traces show the same data at successively higher dispersions by factors of ~10 and finally ending with a 1.0 cm^{-1} segment centered at 1915 cm^{-1}, which corresponds to one of the selected microwindows for NO. Figure 17 shows the entire set of spectra in this microwindow region for this occultation; in fact, the windows depicted in both Fig. 16 and Fig. 17 differ from the nominal microwindow in that in neither case have the solar features been ratioed out and, in the case of Fig. 17, the spectral interval is somewhat wider. This has been done intentionally to illustrate the very different growth characteristics between the NO lines and the water vapor lines identified in the figures, together with the constant absorption

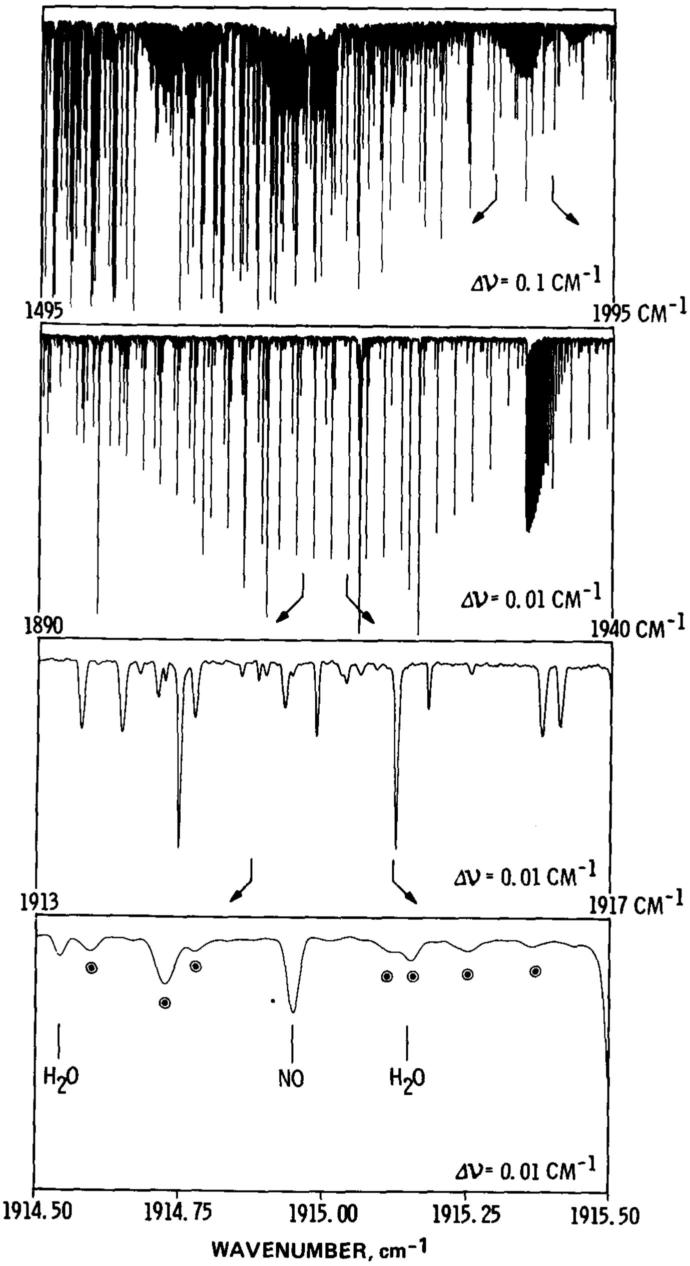

Fig. 16. The top trace in this figure shows a 500 cm^{-1} region of spectrum between 1495 and 1995 cm^{-1} recorded with filter 2. The second trace shows an expanded view of the 1900-1950 cm^{-1} region from the first, the third 4 cm^{-1} similarly expanded from the second in the 1913-1917 cm^{-1} region, and finally 1 cm^{-1} expanded from the third trace centered on 1915 cm^{-1}. This one wavenumber region represents one of the selected microwindows for NO.

characteristics of solar lines. The ATMOS Science Team members selected suitable microwindow regions prior to the SL-3 flight using the best distribution estimates available at the time for each molecule, a standard physical model of the atmosphere, and synthetic spectra generated with the aid of a 150-layer model atmosphere program. To analyze the actual flight

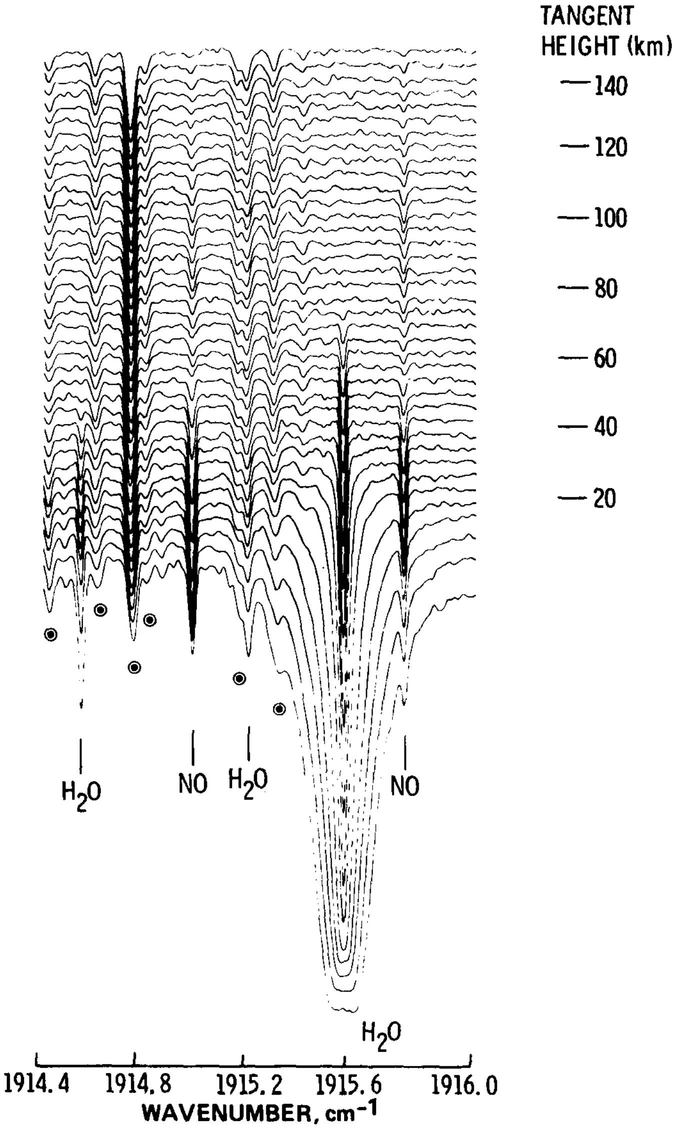

Fig. 17. Shown in this figure is a set of 1.5 cm^{-1} spectral excerpts approximating the NO microwindow shown in Fig. 16. For the purpose of clarity, the spectra have been offset as a function of altitude. Several solar lines and lines of telluric origin are present in the window, in addition to the two lines for NO at 1914.99 and 1915.77 cm^{-1}.

spectra, a program called Occultation Display Spectra (ODS) was created that automatically extracts from the data the microwindows specified by the user and displays them—three successive spectra at a time—on the computer terminal screen. Starting at the highest altitude desired, the user can then activate automatic features of the program that create and iterate synthetic spectra to fit the spectral features contained in the microwindow and proceed downward (in tangent altitude) in "onion-peel" fashion until a concentration profile for the species of interest is derived as a function of altitude. In general, several microwindows are used to derive separate profiles for a given species in each occultation, the individual profiles then being averaged to improve the accuracy of the final result.

The spectroscopic information necessary for generating the synthetic spectra with which the real spectra are compared is contained in two linelists that are maintained by the ATMOS cadre personnel at the DAF and are collectively referred to as the "ATMOS Linelist." The main part of this list contains data based on formal (published) analyses of laboratory spectra with well-established accuracies. A supplemental list contains spectroscopic parameters of varying degrees of accuracy that have not yet been published but nevertheless represent the best data available for several of the trace gases in the stratosphere. Figure 18 shows the regions in both the main (solid

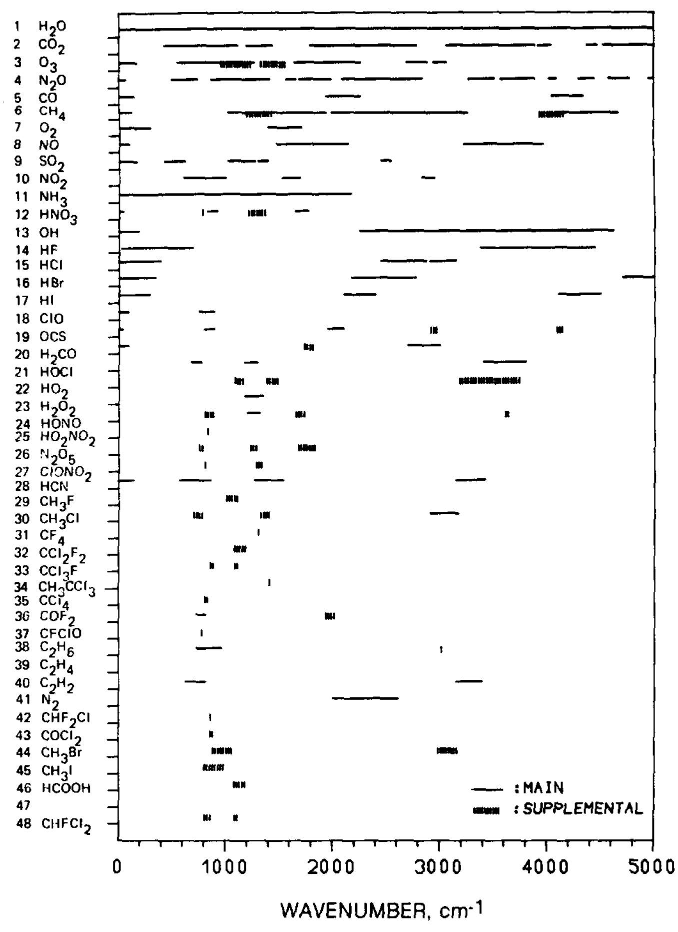

Fig. 18. Summary of the contents of the ATMOS linelists by molecule for the 0 to 5000 cm^{-1} region of the infrared spectrum. Parameters in the main and supplemental linelists are indicated by the solid and hashed lines, respectively.

lines) and supplemental (hashed lines) linelists containing spectroscopic information for the molecules of interest to the ATMOS investigation.

Because of the magnitude of the spectral data sets that can be obtained from an instrument of this type, a large body of additional software has been written to facilitate the ATMOS data analysis activities, including programs for displaying and manipulating real and synthetic spectra, the atmospheric physical and chemical models, and the linelists mentioned above. Both on-line and off-line plotting programs and devices are available for hard-copy graphical presentations of the data. All the spectral examples shown in this report were reproduced directly from the output of these peripheral devices.

Section VII
Results

Representative examples of the ATMOS spectra illustrating the quality of the data and a few of the many interesting spectral features observed are shown in Figs. 19 through 24. Figure 25 is a diagrammatic summary indicating the vertical range of detection for those species whose profiles have been extracted from the data. Notable among the results obtained from the initial examination and analysis of the spectra are the detection of several trace species that had not been observed previously (namely COF_2, N_2O_5, and HNO_4), the confirmation of the presence of $ClONO_2$ in the stratosphere through the identification of five separate vibration-rotation bands, and the first measurement by remote sensing techniques of the principal natural halocarbon, CH_3Cl. A summary of the principal achievements from the SL-3 flight is given in Table 4.

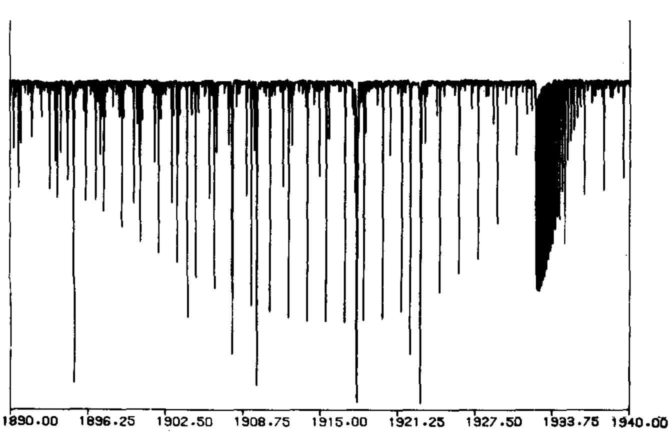

Fig. 19. The P and Q branches of an overtone band of CO_2 as seen from SL-3.

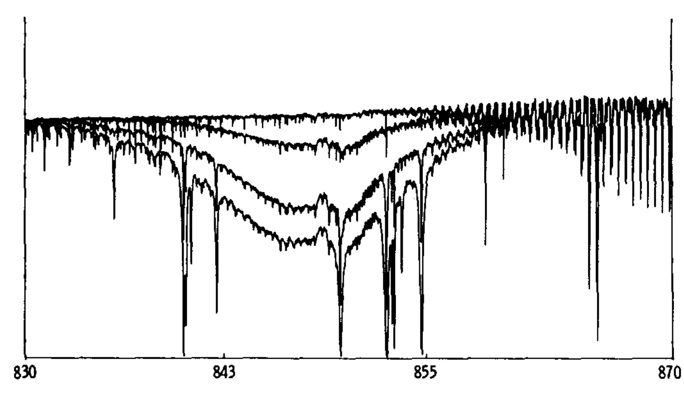

Fig. 20. Portions of four spectra in the region of 830–870 cm^{-1} showing a large unresolved spectral feature of Freon 11 (F-11) in the lower three traces. The lowermost trace in the figure was made at 5 km altitude, and demonstrates that useful tropospheric information can be acquired using this remote sensing technique when atmospheric conditions are favorable. Such conditions prevailed for many of the ATMOS occultations.

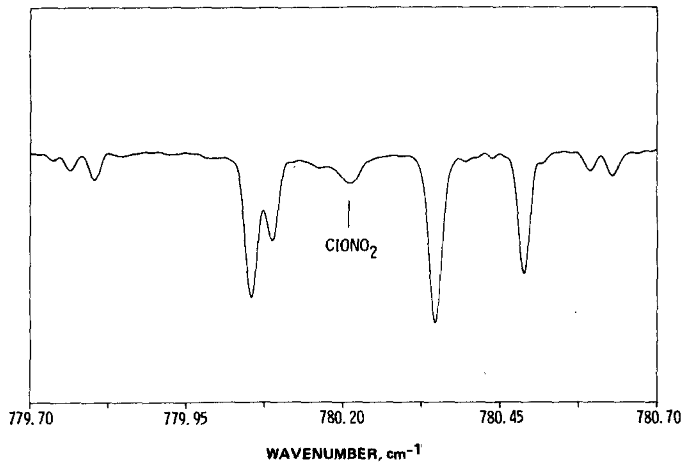

Fig. 21. A portion of the ATMOS spectrum showing the feature of $ClONO_2$ at 780.22 cm^{-1}. This figure illustrates one of the marked advantages of acquiring spectra in large sets such as that returned from SL-3. The spectrum shown, as well as the others used in retrieving the $ClONO_2$ profile, are zonal averages of several spectra from occultations in the same latitudinal regions using the same optical filter and covering the same altitude range. Such averaging can enhance the signal-to-noise characteristics, causing otherwise marginal features to stand out in the data and permitting profiles of concentration to be obtained at only minimum costs in spatial resolution.

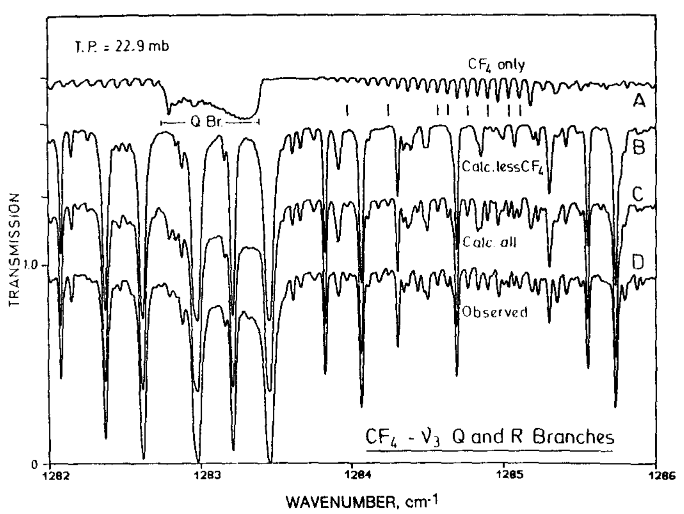

Fig. 22. This figure illustrates how synthetic spectra are used in testing for the presence of a given species in the ATMOS spectra. As indicated, traces A, B, and C are calculated spectra, and the proof of the presence of CF_4 in the real spectrum (trace D) lies in the comparison of D with C.

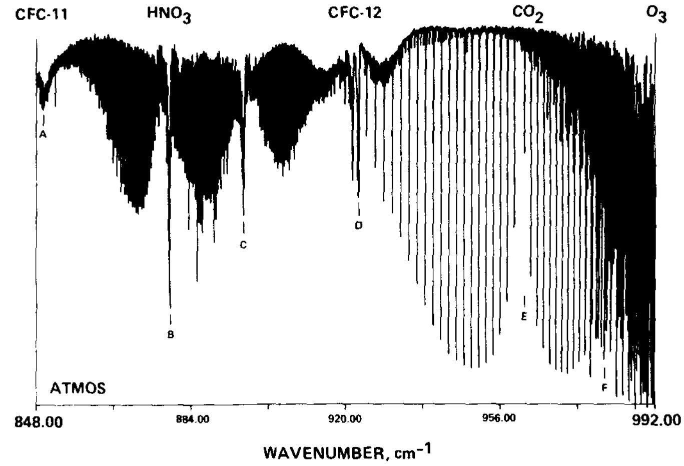

Fig. 23. The feature marked by A in this figure is that of F-11 previously shown in Fig. 20. The features whose Q branches are marked by B and C, respectively, are two transitions of HNO_3; the region between B and C is characterized by perturbations and blendings between the R branch lines of one feature and the P branch lines of the other. D marks the Q-branch of an F-12 absorption feature whose rotational lines are so densely packed they are completely unresolved at the ATMOS resolution, resulting in P and R branches which appear only as depressions in the continuum. E marks the center of a CO_2 absorption characterized by deep (although for CO_2 this is actually a weak transition), relatively widely spaced rotational lines. Beyond F, tightly packed lines of ozone begin to dominate the spectrum.

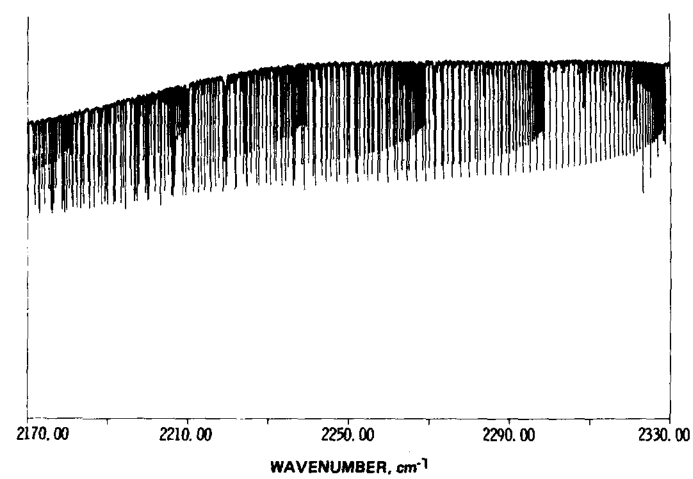

Fig. 24. The outstanding features in this figure are the band heads resulting from transitions between the higher vibration states of CO with $\Delta v = 1$. These features are not seen in telluric spectra, but are solar in nature and occur in the photosphere of the Sun as a result of the high temperatures present in the region. Note the classical folding back of the lines in the band heads at the higher values of J.

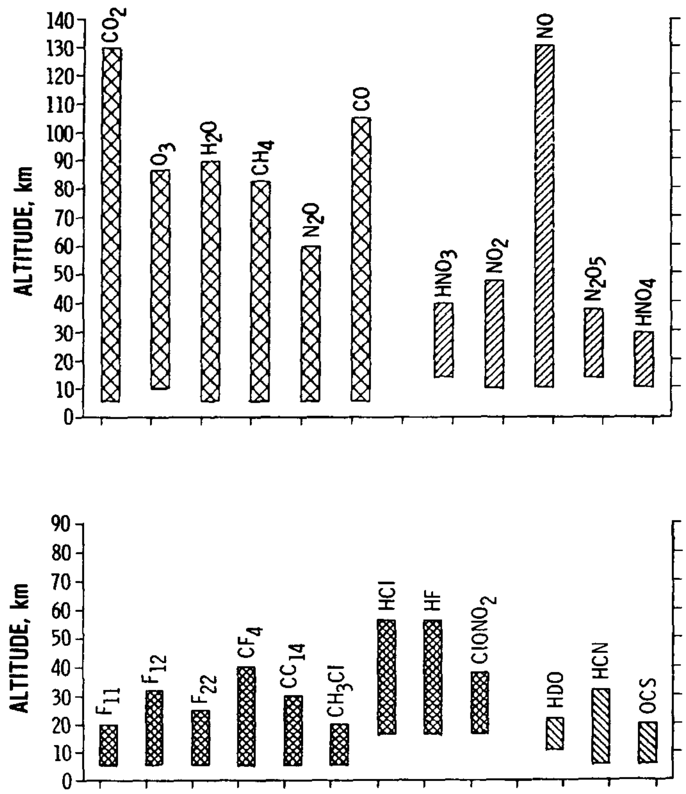

Fig. 25. Diagrammatic summary of species derived from the ATMOS spectra, separated into the minor gases and chemical families of trace species; the bars indicate the altitude ranges over which profiles of concentration can be retrieved from the data.

Table 4. Some of the principal achievements of ATMOS on SL-3.

"Self-contained" ability to determine temperature, pressure, and molecular concentrations.
Concentration profiles for 25 different constituents in the altitude range from the surface to 140 km.
Complete NO_x family.
Complete halogen reservoir species.
HCl and HF to the top of the stratosphere (~60 km).
Ozone chemistry in the mesosphere (O_3, H_2O, and temp.).
Detection of N_2O_5, HNO_4, COF_2, $ClNO_3$, (CH_3Cl, CH_3CCl_3).
Zonal wind profiles, 40 to 110 km.

The three catalytic cycles involved in the depletion of stratospheric ozone (commonly referred to as the ClO_x, NO_x, and HO_x cycles) are shown schematically in Figs. 26, 27, and 28. A comparison of these figures with Fig. 25 shows that a significant number of the source and sink species involved in these cycles were measured by ATMOS in the course of the

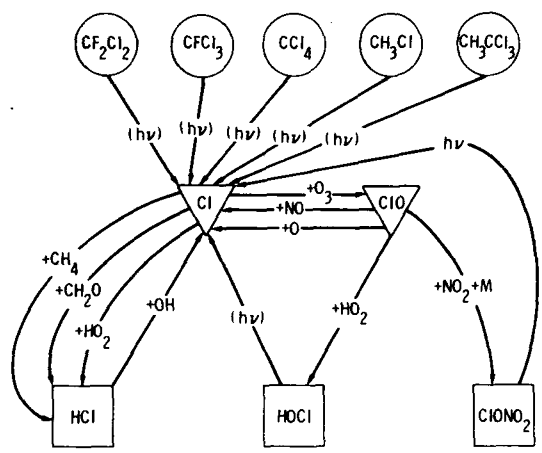

Fig. 26. A schematic representation of the chemical reactions between the ClO_x species and ozone in the stratosphere. In this and the following two figures, circles represent source species, triangles reactive intermediates, and squares represent sinks and reservoirs.

SL-3 investigation. The initial model concentration profiles for the ClO_x, NO_x, and HO_x gases are shown in Figs. 29 through 32, and again these can be compared with the final measured profiles in Figs. 33 through 38. A list of publications, preprints, and manuscripts in preparation detailing all the ATMOS results is given in Appendix I. It is evident that the ATMOS results comprise the most comprehensive set of

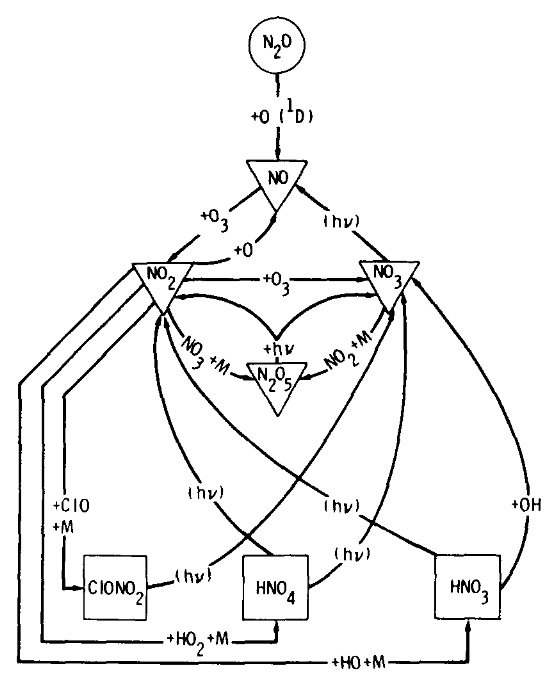

Fig. 27. A schematic similar to Fig. 26 illustrating the $NO_x - O_3$ reactions.

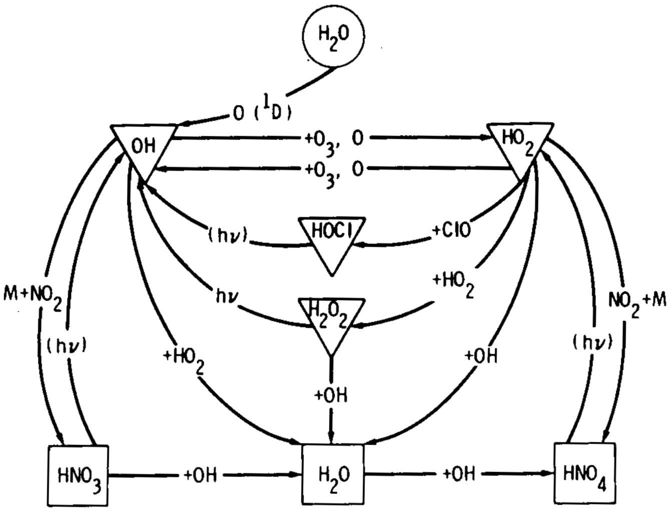

Fig. 28. A schematic similar to Figs. 26 and 27 representing the HO_x chemistry in the stratosphere.

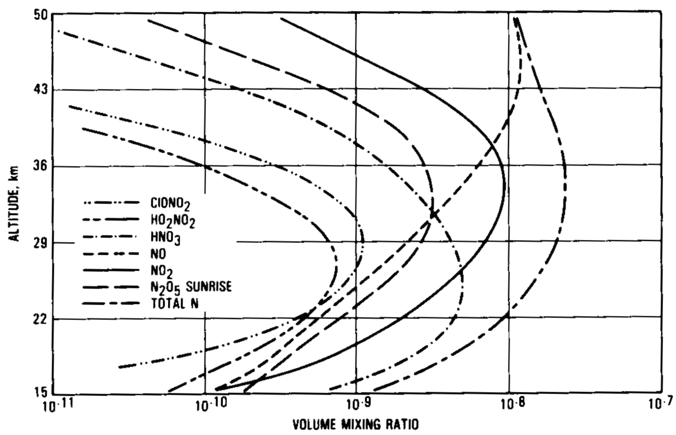

Fig. 31. Model volume mixing ratio profiles as a function of altitude for the NO_x species in the atmosphere.

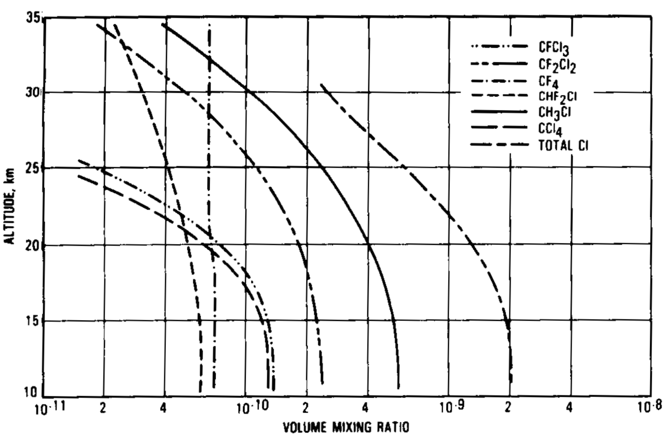

Fig. 29. Model volume mixing ratio profiles as a function of altitude for the halogen source gases in the atmosphere.

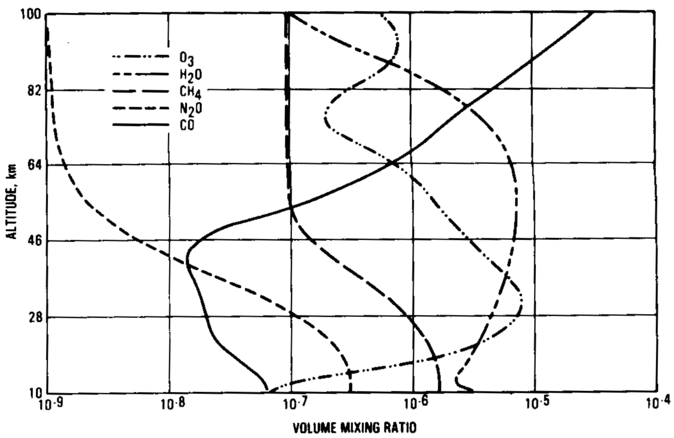

Fig. 32. Model volume mixing ratio profiles as a function of altitude for the minor gases in the atmosphere.

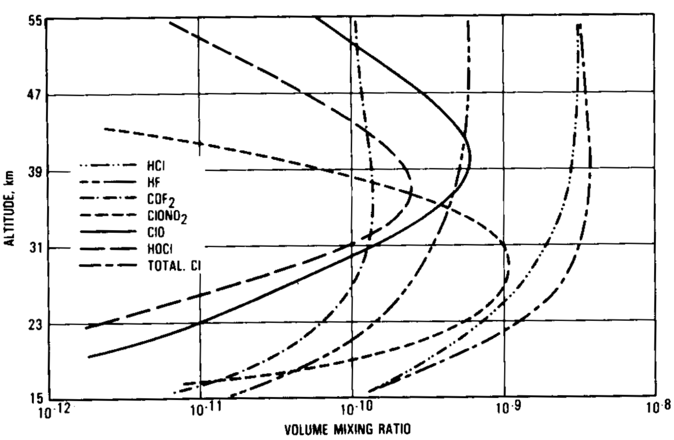

Fig. 30. Model volume mixing ratio profiles as a function of altitude for the halogen sinks and reservoirs in the atmosphere.

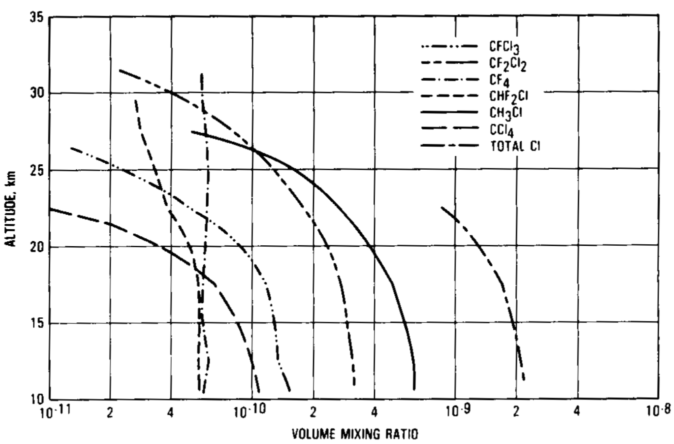

Fig. 33. Halogen source gas profiles as measured by ATMOS in the Northern Hemisphere.

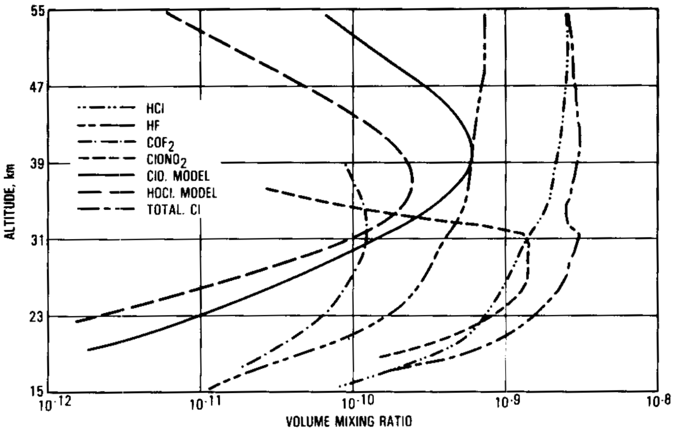

Fig. 34. Halogen sink and reservoir profiles as measured by ATMOS in the Northern Hemisphere. Model profiles for the unmeasured gases of ClO and HOCl have been included in order to calculate the total chlorine.

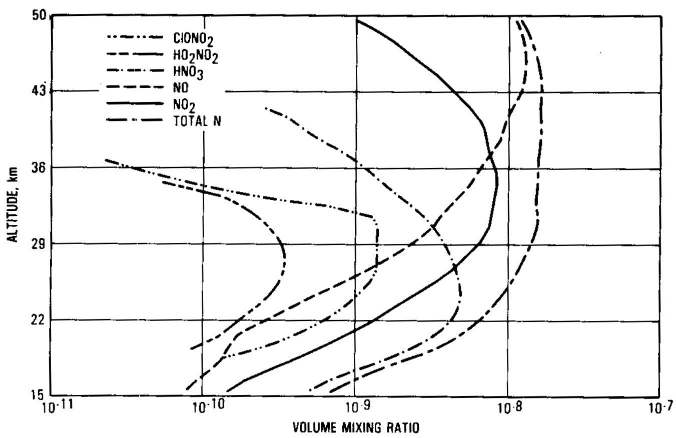

Fig. 35. Profiles for the NO_x species in the atmosphere as measured by ATMOS in the Northern Hemisphere (during sunset).

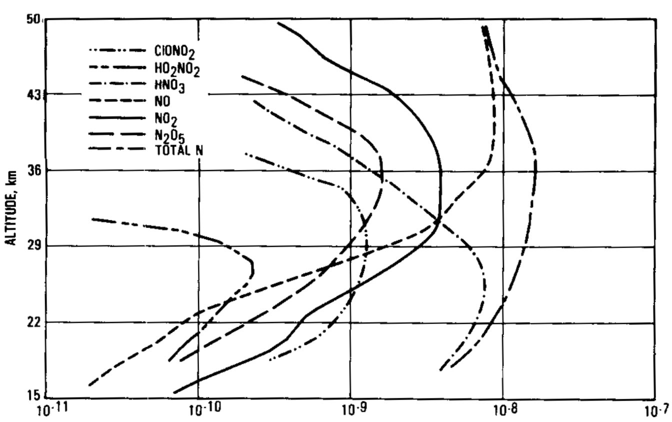

Fig. 36. A set of profiles similar to those in Fig. 35 for Southern Hemisphere sunrises. Note that measurable amounts of N_2O_5 are present at sunrise but not at sunset, as predicted by photochemical models.

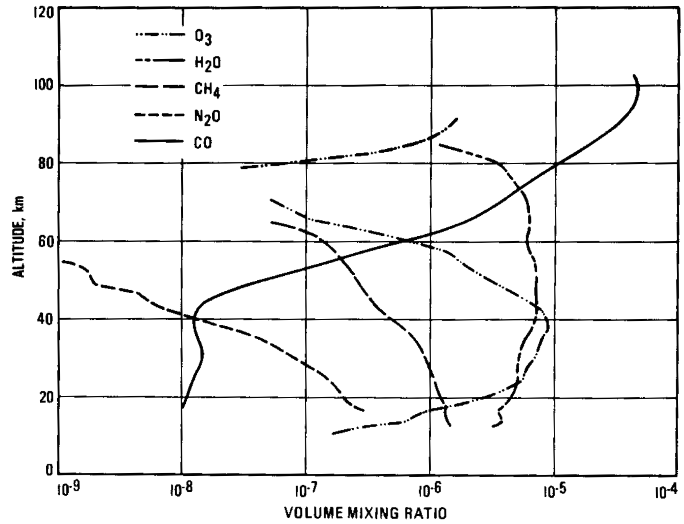

Fig. 37. Atmospheric minor gas profiles as measured by ATMOS at sunrise in the Southern Hemisphere. A discussion of the relationship between the H_2O and CH_4 measurements, mentioned earlier in the text, can be found in the M. Gunson, et al., minor gas paper referenced in Appendix I.

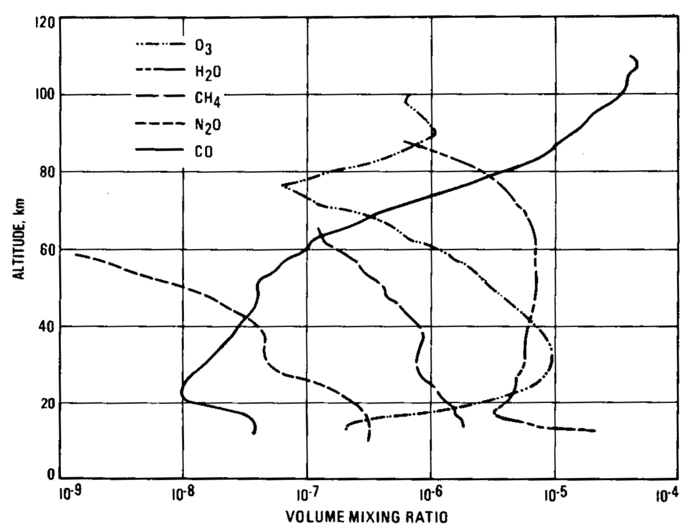

Fig. 38. Atmospheric minor gas profiles as measured by ATMOS at sunset in the Northern Hemisphere.

simultaneously measured upper atmospheric profiles yet obtained. The resolution and sensitivity of the ATMOS instrument is sufficient to allow continuous profiles of concentration for some minor gases (and at least one trace gas) to be determined extending from the upper troposphere through the stratosphere and mesosphere and, in the case of CO_2, CO, and NO, well into the lower thermosphere (i.e., ~130 km). As mentioned earlier, however, the derivation of the profiles in the mesosphere is complicated by the fact that the onset of photochemical thresholds for dissociation and the potential departure from hydrostatic and thermodynamic equilibrium conditions in these regions render invalid many of the assumptions that can be made at lower altitudes to help establish the temperature and pressure environment for the species being measured. Work is continuing by the science team cadre to attempt to unravel the radiative transfer, thermodynamic, photochemical, and transport processes that are occurring in these regions and improve our understanding of the physical conditions at these hitherto uncharted altitudes in our atmosphere.

Section VIII
Future Missions

A. Long-Term Objectives

While the ATMOS flight on SL-3 was conducted in accordance with a comprehensive set of scientific objectives, it can also be viewed as a "proof-of-concept" flight that validated the instrumental and experimental techniques to be used for the long-range objectives of the ATMOS Investigation. ATMOS will be a core part of the Atmospheric Laboratory for Applications and Science (ATLAS) Missions beginning in late 1991 and continuing for a period of at least an 11-year solar cycle, with about one flight per year. Short-range objectives for these missions are expected to be planned on the basis of the current status of upper atmospheric knowledge and the flight conditions for the individual mission opportunities as they arise. The opportunity will be taken to conduct flights at different seasons and inclinations in order to provide the required range of observational parameters for discerning latitudinal and seasonal changes in the upper atmospheric inventory of molecular species. The data from SL-3 will provide an archival record against which the results from later flights can be compared for any long-term changes in the composition of the atmosphere.

B. ATMOS Data Archiving Plan

The SL-3 flight of the ATMOS Investigation was the first in a series of flights that are expected to occur over the next 10 to 15 years, with long-term objectives involving intercomparisons of flight data sets and the participation of guest investigators. As a consequence, the investigation corresponds to the class of missions described in paragraphs 1205.101(c) and 1205.101(d) of NASA Management Instruction 8030.3A, for which it is inappropriate to transfer data to the National Space Science Data Center (NSSDC) after each flight. Instead, a complete listing of all data and data products in every form in which they are available will be furnished the NSSDC, and the appropriate individuals to contact regarding data requests will be identified. In addition, the ATMOS DAF will be made available for the use of interested scientists who wish to avail themselves of both the data and the data analysis programs that are resident in the system. At the end of the extended ATMOS investigation, all the data and supporting documentation then available will be transferred to a more permanent repository at the NSSDC.

To facilitate the acquisition of all the ATMOS profiles of concentration by atmospheric modelers, the NASA Upper Atmospheric Research Office (UARO) has requested that these profiles be made available to the NSSDC in a form that can be easily disseminated to the user community. Accordingly, this information is being furnished to the NSSDC in the form of ASCII files listing constituent concentrations as a function of pressure and altitude on standard floppy disks in a number of formats compatible with most personal computers. A description of each profile and of the conditions and assumptions used in its derivation is contained in each of the ASCII files.

For users interested in the data set itself, the established procedure is to write directly to the ATMOS Principal Investigator at the address shown below stating the areas of interest and requesting that time be made available at the JPL DAF for an initial survey of the appropriate data. Following this, a brief proposal should be submitted to the UARO outlining the research to be done and either requesting further time at the DAF or specific products from the data which are to be furnished to the user. These proposals will be subject to normal peer-review procedures prior to approval if any costs to NASA are involved.

The address of the ATMOS Principal Investigator is:

Dr. C. B. Farmer
MS 183-401
Jet Propulsion Laboratory
4800 Oak Grove Drive
Pasadena, CA 91109

Glossary

AR	Anti-Reflective
ASCII	American National Standard Code for Information Exchange
ATLAS	Atmospheric Laboratory for Applications and Science
ATMOS	Atmospheric Trace Molecule Spectroscopy
BCE	Bench Checkout Equipment
BPI	Bits per Inch
°C	Degrees, Celsius
CCISS	Command and Control Interface Subsystem
CCT	Computer Compatible Tape
CFCs	Chlorofluorocarbons
cm	Centimeter
cm^{-1}	Wavenumber (Reciprocal Centimeter)
cm/s	Centimeter(s) per Second
CPU	Core Processing Unit
DAF	Data Analysis Facility
DHSS	Data Handling Subsystem
EDHSS	Engineering Data Handling Subsystem
EDT	Eastern Daylight Time
EMC	Electromagnetic Compatibility
EMI	Electromagnetic Interference
ESA	European Space Agency
FFT	Fast Fourier Transform
FOV	Field of View
FTP	Fourier Transform Program
GMT	Greenwich Mean Time
GSE	Ground Support Equipment
GSS	Ground Support System
HeNe	Helium-Neon
HEOC	Honeywell Electro-Optics Center
HgCdTe	Mercury-Cadmium-Telluride
HRM	High Rate Multiplexer
HSI	High Speed Interferometer
IPP	Interferogram Processing Program
JPL	Jet Propulsion Laboratory
JSC	Johnson Space Center
K	Kelvin
kbits/s	Kilobits Per Second
KBr	Potassium Bromide
kHz	Kilohertz
km	Kilometer
KSC	Kennedy Space Center
LTE	Local Thermodynamic Equilibrium
LVDT	Linear Variable Differential Transformer
Mbits/s	Megabits Per Second
MCC	Mission Control Center
MET	Mission Elapsed Time
MLI	Multi-Layered Insulation
MPESS	Mission-Peculiar Experiment Support Structure
mr	Milliradian
ms	Millisecond
MSFC	Marshall Space Flight Center
MTL	Master Timeline
NASA	National Aeronautics and Space Administration
NRZ-L	Non-Return to Zero-Logic
NSSDC	National Space Science Data Center
O&C	Operations & Checkout
ODS	Occultation Display Spectra
OPD	Optical Path Difference
OPF	Orbiter Processing Facility
PCM	Pulse Code Modulated
POCC	Payload Operations Control Center
psi	Pounds Per Square Inch
RAM	Random Access Memory
RAU	Remote Acquisition Unit

SAL	Scientific Air Lock
SAM	Shared Access Memory
SEID	Spacelab Experiment Interface Device
SEU	Secondary Electronics Unit
SHSS	Signal Handling Subsystem
SL-1	Spacelab 1
SL-3	Spacelab 3
SOWG	Science Operations Working Group
SST	System/Subsystem Test
STL	Subordinate Timeline
STS	Space Transportation System
TDRSS	Tracking and Data Relay Satellite System
UARO	Upper Atmospheric Research Office
ZnSe	Zinc Selenide

Appendix I

Publication Summary From the ATMOS SL-3 Flight

L. R. Brown, C. B. Farmer, C. P. Rinsland, and R. A. Toth, "Molecular line parameters for the Atmospheric Trace Molecule Spectroscopy (ATMOS) experiment," *Appl. Opt.*, in the press, 1987.

C. B. Farmer, B. Crofton, and O. F. Raper, "High resolution infrared spectroscopy from space: a preliminary report on the results of the Atmospheric Trace Molecule Spectroscopy (ATMOS) experiment on Spacelab 3," *NASA Conference Proceedings*, vol. CP-2429, 1986.

M. R. Gunson, C. B. Farmer, and J. E. Harries, "Upper limits for ATMOS infrared solar absorption spectra," submitted for publication, 1987.

M. R. Gunson, C. B. Farmer, R. H. Norton, R. A. Toth, W. Mankin, C. P. Rinsland, J. Park, J. Shaw, B. C. Gao, L. Gray, F. Taylor, C. Zammit, and R. Zander, "Minor gases in the upper troposphere, stratosphere, and mesosphere measured by ATMOS," in preparation.

R. H. Norton, J. Park, and C. P. Rinsland, "ATMOS data processing and science analysis methods," in preparation.

J. H. Park, R. Zander, C. B. Farmer, C. P. Rinsland, J. M. Russell III, R. H. Norton, and O. F. Raper, "Spectroscopic detection of CH_3Cl in the upper troposphere and lower stratosphere," *Geophys. Res. Lett.*, vol. 13, pp. 765–768, 1986.

O. F. Raper, C. B. Farmer, R. Zander, and J. H. Park, "Infrared spectroscopic measurements of halogenated sink and reservoir gases in the stratosphere from the ATMOS Spacelab 3 mission," *J. Geophys. Res.*, in the press (1987).

C. P. Rinsland, R. Zander, L. Brown, C. B. Farmer, J. H. Park, R. H. Norton, J. M. Russell III, and O. F. Raper, "Detection of carbonyl fluoride in the stratosphere," *Geophys. Res. Lett.*, vol. 13, pp. 769–7672, 1986.

C. P. Rinsland, R. Zander, C. B. Farmer, R. H. Norton, and J. M. Russell III, "Concentrations of ethane (C_2H_6) in the lower stratosphere and the upper troposphere and acetylene (C_2H_2) in the upper troposphere deduced from ATMOS Spacelab 3 spectra," submitted for publication (1987).

C. P. Rinsland, R. Zander, C. B. Farmer, R. H. Norton, L. R. Brown, J. M. Russell III, and J. H. Park, "Evidence for the presence of the 802.7 cm^{-1} band Q branch of the HO_2NO_2 in high resolution absorption spectra of the stratosphere," *Geophys. Res. Lett.*, vol. 13, pp. 761–764, 1986.

J. M. Russell III, C. B. Farmer, C. P. Rinsland, R. Zander, L. Froidevaux, G. C. Toon, B. Gao, and J. Shaw, "Measurements of odd nitrogen compounds in the stratosphere by the ATMOS experiment on Spacelab 3," submitted for publication, (1987).

G. C. Toon, C. B. Farmer, and R. H. Norton, "Detection of stratospheric N_2O_5 by infrared remote sounding," *Nature*, vol. 319, pp. 570–571, 1986.

G. W. Van Cleef, J. H. Shaw, and C. B. Farmer, "Zonal winds between 25 and 120 kilometers obtained from solar occultation spectra," submitted for publication.

R. C. Zander, C. P. Rinsland, C. B. Farmer, L. R. Brown, and R. H. Norton, "Observations of several chlorine nitrate ($ClONO_2$) bands in stratospheric infrared spectra," *Geophys. Res. Lett.*, vol. 13, pp. 757–760, 1986.

R. Zander, C. P. Rinsland, C. B. Farmer, J. Namkung, R. H. Norton, and J. M. Russell III, "Concentrations of carbonyl sulfide (OCS) and hydrogen cyanide (HCN) in the free upper troposphere and lower stratosphere deduced from ATMOS/Spacelab 3 infrared solar occultation spectra," submitted for publication.

R. Zander, C. P. Rinsland, C. B. Farmer, and R. H. Norton, "Infrared Spectroscopic measurements of halogenated source gases in the stratosphere with the ATMOS instrument," *J. Geophys. Res.*, in press (1987).

In addition to the above, manuscripts on the following subjects are in the planning stage:

a. Temperature, pressure, and tangent height retrievals from the ATMOS data.
b. CO_2/CO in the upper atmosphere.
c. CO and NO in the mesosphere.
d. O_3 (668) in the stratosphere.
e. Stratospheric HDO/H_2O ratio.
f. Continuum absorption of N_2, O_2, and H_2O.

Appendix II

ATMOS Master Timeline Sequence

Table II-1. Representative occultation sequence from the ATOMS Spacelab 3 master timeline. Separate subordinate timelines are set off by triple spaces.

Event Table			
DT	Command	Event	Code
T - 10:00	Cooler On	Cooler powered up	$0170
T - 03:05	Run	Instrument in RUN mode	$0477
T - 03:00	Laser On	Laser powered up	$0007
T - 02:50	Camera On	Power up camera	$081A
T - 00:50	Mode Fringe	Select fringe sampling mode	$039E
T - 00:48	Suntracker Enable	Suntracker power on	$055C
T - 00:47	FOV Enable	Enable field of view wheel	$072C
T - 00:45	Uncage	Uncage scan servo	$02C5
T - 00:39	Start Slide	Activate scan servo	$0636
T - 00:38	Suntracker Azimuth	Suntracker positioned for	$OEXY
T - 00:37	Suntracker Elevation	solar acquisition	$0FXY
T - 00:17	Suntracker Offset	Position FOV on solar disk	$10XY
T - 00:16	FOV-1	Select 1 mrad field of view	$0C01
T - 00:07	Optical Filter No. 3	Position optical filter	$0D02
T - 00:06	Gain Setting	Gain state selected	$11XY
T - 00:05	Sample Rate: 2	Sample every 2nd laser fringe	$08AE
T - 00:04	Camera Enable	Bring frame camera on line	$096D
T - 00:00	Sun Acquisition	Sun lock enabled, data acquired	$12EE
T + 03:00	Stop Slide	Turn off scan servo	$062B
T + 03:05	Cage	Cage scan servo	$025B
T + 03:10	Calibrate	Run while caged	$03D8
T + 03:16	Cooler Off	Turn off cooler power	$01A8
T + 03:17	Laser Off	Turn off laser power	$0055
T + 03:18	Stow (az. and elev.)	Suntracker stow	$0B1D
T + 03:19	Sun Presence Disable	Inhibit Sun presence	$12E9
T + 03:20	Camera Disable	Inhibit frame camera	$0962
T + 03:21	FOV Disable	Turn off field of view wheel	$07F7
T + 03:22	Camera Off	Camera power off	$08D8
T + 03:23	Suntracker Disable	Turn off suntracker power	$05C2
T + 04:00	Standby	Instrument power to standby	$04AF

Table II-2. A summary of the entire set of master timeline sequences planned for the ATMOS experiment on SL-3. "SET" and "RISE" represent sunset and sunrise occultations, and "SUNCAL" and "SKYCAL" refer to calibration sequences performed on the high sun or the cold sky.

OBS No.	FO Type	MET (d/hh:mm:ss)	FOV (mr)	Fltr No.	Smpl Rate	Low Gain	Com Gain
1	SET	0/07:14:06	1	3	2	0.5	8
2	SET	0/08:07:42	2	1	2	0.5	8
3	SET	1/07:01:47	1	3	2	0.5	8
4	SET	1/08:33:34	2	2	2	0.5	4
5	SET	1/10:05:11	2	1	2	0.5	8
6	RISE	1/15:17:40	1	4	3	0.5	8
7	RISE	1/16:49:16	2	2	2	0.5	4
8	RISE	1/18:20:52	2	1	2	0.5	8
9	RISE	1/19:52:28	1	5	2	1.0	8
10	SET	2/01:21:24	1	3	2	0.5	8
11	SET	2/02:53:02	1	4	3	0.5	8
12	SET	2/04:24:39	1	3	2	0.5	8
13	SET	2/05:56:17	2	2	2	0.5	4
14	SET	2/07:27:54	1	3	2	0.5	8
15	SET	2/08:59:32	2	1	2	0.5	8
16	RISE	2/14:11:43	1	3	2	0.5	8
17	RISE	2/15:43:19	1	4	3	0.5	8
18	RISE	2/17:14:56	1	3	2	0.5	8
19	RISE	2/18:46:32	1	5	2	1.0	8
20	RISE	2/20:18:09	1	3	2	0.5	8
21	SET	3/00:15:48	1	3	2	0.5	8
22	SET	3/01:47:26	1	4	3	0.5	8
23	SET	3/03:19:04	1	3	2	0.5	8
24	RISE	3/04:50:42	2	2	2	0.5	4
25	SET	3/06:22:20	1	3	2	0.5	8
26	SET	3/07:53:58	2	1	2	0.5	8
27	SET	3/09:25:36	1	3	2	0.5	8
28	RISE	3/14:37:28	1	3	2	0.5	8
29	RISE	3/16:09:04	2	2	2	0.5	4
30	RISE	3/17:40:41	1	3	2	0.5	8
31	RISE	3/19:12:18	2	1	2	0.5	8
32	RISE	3/20:43:55	1	3	2	0.5	8
33	SET	4/02:13:34	2	1	2	0.5	8
34	SET	4/03:45:13	1	3	2	0.5	8
35	SET	4/05:16:51	2	2	2	0.5	4
36	SET	4/06:48:29	1	3	2	0.5	8
37	SET	4/08:20:07	2	1	2	0.5	8
38	SET	4/09:51:45	2	2	2	0.5	4
39	RISE	4/15:03:18	1	3	2	0.5	8
40	RISE	4/16:34:55	2	2	2	0.5	4
41	SET	4/17:29:57	1	5	2	1.0	8
42	RISE	4/18:06:33	1	3	2	0.5	8
43	RISE	4/19:38:10	2	1	2	0.5	8
44	SET	4/23:36:31	1	5	2	1.0	8
45	SET	5/01:08:09	1	4	3	0.5	8
46	SET	5/03:39:48	1	3	2	0.5	8
47	SET	5/04:11:26	2	2	2	0.5	4
48	SET	5/05:43:05	1	3	2	0.5	8
49	SET	5/07:14:43	2	1	2	0.5	8

Table II-2 (contd)

OBS No.	FO Type	MET (d/hh:mm:ss)	FOV (mr)	Fltr No.	Smpl Rate	Low Gain	Com Gain
50	RISE	5/13:57:38	1	4	3	0.5	8
51	RISE	5/15:29:16	1	3	2	0.5	8
52	RISE	5/17:00:53	2	2	2	0.5	4
53	RISE	5/18:32:31	1	3	2	0.5	8
54	RISE	5/20:04:08	2	1	2	0.5	8
55	SET	6/00:02:48	1	3	2	0.5	8
56	SET	6/01:34:26	1	4	3	0.5	8
57	SET	6/03:06:05	1	3	2	0.5	8
58	SET	6/04:37:44	2	2	2	0.5	4
59	SET	6/06:09:22	1	3	2	0.5	8
60	SET	6/07:41:01	2	1	2	0.5	8
1	SUNCAL	0/06:23:00	1-2	1-6	2-3	0.5-1	4-8
2	SUNCAL	0/08:02:42	1-2	1-6	2-3	0.5-1	4-8
3	SUNCAL	1/16:55:26	1	6	2	0.5	8
4	SUNCAL	2/05:51:46	1	4	3	0.5	8
5	SUNCAL	2/15:49:29	1	6	2	0.5	8
6	SUNCAL	3/06:17:41	1	4	3	0.5	8
7	SUNCAL	3/16:15:14	1	6	2	0.5	8
8	SUNCAL	4/06:43:29	1	4	3	0.5	8
9	SUNCAL	4/16:41:05	1	6	2	0.5	8
10	SUNCAL	5/07:09:43	1	4	3	0.5	8
11	SUNCAL	6/17:07:03	6	1	2	0.5	8
1	SKYCAL	1/07:06:46	1	6	2	0.5	8
2	SKYCAL	6/01:41:25	1	6	2	0.5	8

TECHNICAL REPORT STANDARD TITLE PAGE

1. Report No. JPL Pub. 87-32	2. Government Accession No.	3. Recipient's Catalog No.
4. Title and Subtitle Final Report on the First Flight of the ATMOS Instrument During the Spacelab 3 Mission, April 29 Through May 6, 1985		5. Report Date October 1, 1987 6. Performing Organization Code
7. Author(s) Crofton B. Farmer, et al.		8. Performing Organization Report No.
9. Performing Organization Name and Address JET PROPULSION LABORATORY California Institute of Technology 4800 Oak Grove Drive Pasadena, California 91109		10. Work Unit No. 11. Contract or Grant No. NAS7-918 13. Type of Report and Period Covered JPL Publication
12. Sponsoring Agency Name and Address NATIONAL AERONAUTICS AND SPACE ADMINISTRATION Washington, D.C. 20546		14. Sponsoring Agency Code RE4 BP-618-41-00-03-02

15. Supplementary Notes

16. Abstract

The underlying rationale and the implementation of the Atmospheric Trace Molecule Spectroscopy (ATMOS) investigation are discussed, a description of the sensor is given, and the ground tests and integration procedures leading to the Spacelab 3 flight are described. The data reduction and analysis procedures used after the flight are discussed, a number of examples of the spectra obtained are shown, and the concentration profiles as a function of altitude for the minor and trace gases measured during the mission are presented.

On the basis of the instrument's ability to survive both the launch and the reentry of the shuttle and its flawless performance while on orbit, the concepts involved in the investigation have been proved by the Spacelab 3 flight, and an extended series of reflights are currently being planned as a part of the Atmospheric Laboratory for Applications and Science (ATLAS) Missions. The goals for the investigation during these missions are also discussed.

IN-43-CR
115283
50P.

17. Key Words (Selected by Author(s)) Earth Resources Environment Pollution Geochemistry Solar Physics	18. Distribution Statement Unlimited

19. Security Classif. (of this report)	20. Security Classif. (of this page)	21. No. of Pages	22. Price
Unclassified	Unclassified	vii + 45	

JPL 0184 R 9/83